*Archives of Hydro-Engineering and Environmental Mechanics*
Vol. 41 (1994), No. 1–2, pp. 37–84

# Random Water Wave Kinematics
# Part 2. Experiment

**Witold Cieślikiewicz*, Ove T. Gudmestad****

* Institute of Hydro-Engineering, PAS, Gdańsk, Poland
** Statoil, Stavanger, Norway

(Received May 10, 1993; revised August 9, 1993)

**Abstract**

In this work measured wave flume kinematics data are compared with the non-linear theory of random waves, which is presented in Part 1 of this paper (Cieślikiewicz, Gudmestad 1994). Conformity of theory and the experiment is excellent. The only difference between predictions and measurements was found in the mean value of the horizontal velocity. It is suggested in this study, that the existence of the return flow in a confined wave flume explains the deviation. The theoretical results of Part 1 are therefore used for better estimation of that return current.

## 1. Introduction

If we assume that a random wave is a composition of denumerably many independent harmonic components, then by the central-limit theorem the free surface elevation becomes Gaussian. The Gaussian model, however, inherits all the difficulties of the linear wave theory. This is particulary evident in the surface zone. For example, one difficulty relates to finding the probability law for the water particle velocity at a point in the vicinity of the mean water level. In actual waves, this point would sometimes be above the sea surface and sometimes below it. The velocity would assume a range of values when the point was submerged and would not be determined (or set to be zero by assumption) when not submerged. In Part 1 of this paper the possible answer to the above question has been presented. The water wave velocities, modified by the so-called *emergence effect*, were examined and stochastic characteristics of that random field were determined. It is evident that the velocities at points near the surface zone follow a non-Gaussian distribution even under the assumption that the sea surface oscillations are Gaussian. This is so, since the relation between the surface elevation and the modified velocity is non-linear even when the relation between the elevation and the unmodified velocity is linearized. Hence, we discuss the kind of non-linear effects that exist in the framework of linear wave theory.

In the theoretical considerations of Part 1, in addition to the emergence effect, the influence of non-linearity of the motion itself was examined. The aim of Part 2 of this paper is, firstly, to check, basing on measurements, the validity of the approach to surface effects by introducing the emergence effect. Secondly, to compare the influence of that effect with the influence on wave kinematics of second-order wave theory non-linearities.

There are not many papers reporting particle velocity measurements with emphasis given to measurements in the vicinity of the mean water level. First such an experiment was reported by Anastasiou *et al.* (1982a, b), and recently, by Skjelbreia *et al.* (1989, 1991). These latter measurements will be used to verify the theoretical findings of this study. The results have recently been used to update random wave velocity estimates (Gudmestad and Haver 1993).

## 2. Experimental Setup

The experimental arrangement and subsequent results discussed below were described in detail in papers by Skjelbreia *et al.* (1989, 1991). The experiments were carried out in a tank which is 33 m long, 1.02 m wide and 1.8 m deep. The irregular wave generator of this tank is hydraulically driven and the control signal was constructed from a JONSWAP target wave spectrum using JONSWAP peakedness factor $\gamma = 3.0$. The spectrum was divided into 1 000 frequency components and each component had a random phase.

At the end of the tank, opposite the wave generator, was located a passive wave absorber consisting of a series of vertical perforated steel plates. The reflection coefficient was estimated as $\approx 5\%$ over a broad frequency range.

The surface elevation for each wave case studied by Skjelbreia *et al.* (1989, 1991) was generated from one spectrum and measured with 7 standard resistive-type gauges. The special arrangement of the gauges was adopted to decompose incoming and reflected irregular waves (Zelt and Skjelbreia 1992). Three gauges were placed close to each other in order to resolve the first order waves, while another four gauges were distributed along the wave tank to resolve long waves. The accuracy of the wave gauge positions was 0.01 m.

The flow velocity was measured on the centreline at a single longitudinal position along the tank, coinciding with one of the gauges, but at several different elevations by a two-component Laser Doppler Velocimeter (LDV). The two velocity components were measured in a plane parallel to the side wall of the tank with a measurement volume cross-section of approximately 100 $\mu$m in diameter. The LDV was specifically designed for this study and had the special feature of using only a single laser beam in the flow.

The LDV allowed measurements from wave crest down to tank bottom but at one point in space only during one run. In order to obtain the distributions for the statistical properties of the velocity along the vertical axis it was necessary to

repeat the experiment with exactly the same free surface elevation spectrum but locating the LDV station at different vertical positions. Great care was therefore given to maintain reproducible wave conditions in the tank. It was found that it is very important for reproducibility of the wave flow to keep a constant water depth. Special attention was paid to measuring orbital velocity components within the surface layer.

Each run in the test programme had a duration of 819.2 s. All seven wave gauge channels were sampled simultaneously with the two LDV channels, at a rate of 40 Hz.

## 3. Statistical Analysis of Measured Free Surface Elevation and Particle Kinematics

In order to examine the variation of the stochastic properties of velocities with $z$-elevation, the analysis of a number of runs for two wave cases from Skjelbreia's measurements in the Norwegian Hydrotechnical Laboratories' wave tank (Skjelbreia *et al.* 1989, 1991) was carried out. These were 12 runs of Case 5—measurements series I18 and 13 runs of Case 6—measurements series I24. The wave conditions reproduced in the tank for *selected sea states* were given by the significant wave heights $H_S$ and the peak periods $T_p$ as presented in Table 1. The measurement levels for each run as well as statistical properties of surface elevation are listed in Tables 2 and 3 for Cases 5 and 6, respectively.

**Table 1.** Wave parameters for cases analysed (Skjelbreia *et al.* 1989, 1991)

| Wave Case | Measurement Series | $H_S$ (m) | $T_p$ (s) | Depth (m) |
|---|---|---|---|---|
| 5 | I18 | 0.21 | 1.8 | 1.3 |
| 6 | I24 | 0.25 | 2.4 | 1.3 |

Digitizations of the free surface elevation and velocity time series were carried out at a rate of 40 Hz and samples of 32 768 measuring points were collected. The first 2048 and last 1024 data points for each time series were omitted in order to cancel possible transition effects, giving finally the $N = 29\,696$ point length sequence.

Measurements of the particle velocity near the mean water level have varying degrees of intermittency behaviour depending upon the level at which they were obtained. This occurs when the probe volume of the LDV emerges from the water. Until the water surface moves back up to the level of the LDV the signal holds at the last measured value (Skjelbreia *et al.* 1989). Figure 1 shows this behaviour of recorded velocities. Time series of particle velocities $u_i$ and $w_i$ were therefore modified numerically such that their values during *drop-out* periods were set equal

to zero:

$$[\bar{u}_i, \bar{w}_i] = [u_i, w_i]\mathcal{H}(\zeta_i - z) \tag{1}$$

in which $z$ is the level of the LDV and $\mathcal{H}(\cdot)$ is the Heaviside unit step function. In the last equation, and below in this chapter, the notation has been changed for convenience. Namely, subscript indicates the number of data point in the sample, while the velocity components are $u, v, w$, i.e. $\mathbf{u} = [u, v, w]$ and $\bar{\mathbf{u}} = [\bar{u}, \bar{v}, \bar{w}]$. Equation (1) is of course in agreement with the equation (5)*.[1]

The time series $\zeta_i$, $\bar{u}_i$ and $\bar{w}_i$ were subjected to statistical and spectral analysis. The statistical analysis involved calculation of the first four statistical moments, coefficients of skewness and kurtosis and probability density functions for each series. Also joint statistical moments for surface elevation and orbital velocities were calculated. In this section spectral analysis results of the data are presented while those concerning probability distributions will be discussed in the next section.

Figures 2 a, b, c illustrate the character of the time series $\zeta_i$, $\bar{u}_i$ and $\bar{w}_i$ for various vertical locations of the LDV station. It is clearly seen that the emergence effect becomes more pronounced for higher LDV elevations.

Segmental smoothing was required for the spectral calculations. This was done according to the "Welch method" (Oppenheim and Schafer 1975). The sequences of length $N = 29\,696$ points were divided into 57 sections of $M = 1\,024$ points each. The segments were overlapped by one half of their length. Successive sections were multiplied by a Hanning window, transformed with a 1 024-point FFT, summed and averaged. This smoothing resulted in a number of degrees of freedom equal to double the number of sections the sequence was divided into, i.e. 114. The 95% confidence intervals were estimated by calculating the variance of the unaveraged spectral estimates under the assumption of normal distribution.

The power spectra for 513 frequency values evenly spaced between 0 and the Nyquist frequency ($f_c = 20$ Hz) were obtained. For the analysed wave case the peak frequency $f_p \approx 0.56$ Hz, and for the most energetic range $(0, 3f_p)$ 43 values of the power spectra were obtained with discrete frequency spacing $\Delta f = 0.039$ Hz ( $\Delta\omega = 0.245$ rad/sec). In addition, coherence and transfer function estimates were obtained from cross-spectral estimates between surface elevation and velocities:

$$T_{\zeta\bar{u}}(\omega) = \frac{S_{\zeta\bar{u}}(\omega)}{S_{\zeta\zeta}(\omega)}, \qquad T_{\zeta\bar{w}}(\omega) = \frac{S_{\zeta\bar{w}}(\omega)}{S_{\zeta\zeta}(\omega)}, \tag{2}$$

$$\gamma^2_{\zeta\bar{u}}(\omega) = \frac{|S_{\zeta\bar{u}}(\omega)|^2}{S_{\zeta\zeta}(\omega)S_{\bar{u}\bar{u}}(\omega)}, \quad \gamma^2_{\zeta\bar{w}}(\omega) = \frac{|S_{\zeta\bar{w}}(\omega)|^2}{S_{\zeta\zeta}(\omega)S_{\bar{w}\bar{w}}(\omega)}, \tag{3}$$

where $S_{\zeta\zeta}$, $S_{\bar{u}\bar{u}}$, $S_{\bar{w}\bar{w}}$ are spectral densities for $\zeta$, $\bar{u}$ and $\bar{w}$ respectively, $S_{\zeta\cdot}$ are the cross-spectral densities between surface elevation and velocities, $T_{\zeta\cdot}$ are the

[1] We use a star * to denote equation numbers in Part 1 of this paper.

complex transfer functions from $\zeta$ to velocity marked in subscript, and $\gamma^2_{\zeta\cdot}$ are the corresponding coherence functions.

The measured spectra of surface elevation were used to calculate the statistical parameters for the particle kinematics (Section 4). These calculations involve numerical integration over frequency. In order to obtain integrals with high accuracy and with a small number of function evaluations of the integrand, the adaptive recursive Gaussian quadrature method was used. Cubic spline interpolation was used to prepare the suitable function segments for the computer programme. Spectral densities, coherences and transfer functions presented in the following figures were also interpolated over a finer abscissa using cubic splines.

Figures 3 and 4 show estimated spectral densities of surface elevation $\zeta$ for Run 1 of Case 5 and Run 6 of Case 6. It is noted that the measured spectra show no obvious secondary peaks. Cases with higher degrees of non-linearity were not available from Skjelbreia's series of experiments. It should be noted that very good reproducibility of wave conditions was obtained in the tank—at least when spectral density of surface elevation was considered. Deeper insight into this question gives examination of the first four statistical moments of free surface elevation. In Tables 2 and 3 the mean values, standard deviations, skewness and kurtosis coefficients are presented for the 12 runs of wave Case 5 (I18) and 13 runs of Case 6 (I24). Skewness is not much greater than 0.2 for each of them, which means that strong deviations from the Gaussian distribution (Ochi and Wang 1984) should not be expected for the free surface.

In Figure 5 the histograms with 30 equally spaced bins between the minimum and maximum values of $\zeta$ for Run 10 of Case 5 and Run 16 of Case 6 are presented, showing the estimated probability distribution of free surface elevation. Values $p_i$ of the histogram are scaled so that direct comparison with probability density function is possible:

$$p_i = \frac{n_i}{N\Delta_\zeta} \quad \text{for } i = 1, 2, \ldots, 30, \tag{4}$$

in which $N$ is the number of data points (29 696 in this example), $n_i$ is the number of data points observed in the $i$th bin and $\Delta_\zeta$ is the width of the bin. Outliers greater than 5 standard deviations were removed which gave the bin's width $\Delta_\zeta \leq \sigma_\zeta/3$.

It is seen from Figure 5 that measured surface elevations only slightly deviate from the Gaussian distribution. This means that for points which are continuously submerged we should not expect significant deviations from the linear wave theory in both wave cases analysed.

Figures 6 to 13 show observed spectral densities of horizontal and vertical velocities as well as transfer and coherence functions between $\zeta$ and velocities for Case 5, while Figures 14 to 21 show the same quantities for Case 6. Three elevations are considered for the horizontal velocity while results for the vertical

**Table 2.** LDV locations and statistical properties of surface elevation for Case 5 runs analysed

| Run | Measurement level $z$ (m) | Statistical properties of surface elevation | | | |
|---|---|---|---|---|---|
| | | Mean value (m) | Standard deviation (m) | Skewness | Kurtosis −3 |
| 30 | 0.20 | $-1.69 \cdot 10^{-3}$ | $5.387 \cdot 10^{-2}$ | $2.59 \cdot 10^{-1}$ | $1.78 \cdot 10^{-1}$ |
| 27 | 0.15 | $-2.00 \cdot 10^{-3}$ | $5.488 \cdot 10^{-2}$ | $2.50 \cdot 10^{-1}$ | $1.64 \cdot 10^{-1}$ |
| 15 | 0.10 | $-2.08 \cdot 10^{-3}$ | $5.675 \cdot 10^{-2}$ | $2.65 \cdot 10^{-1}$ | $1.50 \cdot 10^{-1}$ |
| 10 | 0.05 | $-2.17 \cdot 10^{-3}$ | $5.410 \cdot 10^{-2}$ | $2.46 \cdot 10^{-1}$ | $1.66 \cdot 10^{-1}$ |
| 25 | 0.00 | $-1.28 \cdot 10^{-3}$ | $5.334 \cdot 10^{-2}$ | $2.49 \cdot 10^{-1}$ | $1.78 \cdot 10^{-1}$ |
| 23 | −0.05 | $-1.36 \cdot 10^{-3}$ | $5.464 \cdot 10^{-2}$ | $2.62 \cdot 10^{-1}$ | $1.64 \cdot 10^{-1}$ |
| 1 | −0.10 | $-1.99 \cdot 10^{-3}$ | $5.340 \cdot 10^{-2}$ | $2.41 \cdot 10^{-1}$ | $2.24 \cdot 10^{-1}$ |
| 7 | −0.20 | $-2.33 \cdot 10^{-3}$ | $5.395 \cdot 10^{-2}$ | $2.48 \cdot 10^{-1}$ | $1.85 \cdot 10^{-1}$ |
| 16 | −0.25 | $-1.99 \cdot 10^{-3}$ | $5.645 \cdot 10^{-2}$ | $2.67 \cdot 10^{-1}$ | $1.50 \cdot 10^{-1}$ |
| 18 | −0.50 | $-4.18 \cdot 10^{-3}$ | $5.361 \cdot 10^{-2}$ | $2.55 \cdot 10^{-1}$ | $1.97 \cdot 10^{-1}$ |
| 20 | −1.00 | $-3.09 \cdot 10^{-3}$ | $5.335 \cdot 10^{-2}$ | $2.47 \cdot 10^{-1}$ | $2.29 \cdot 10^{-1}$ |
| 34 | −1.105 | $-2.50 \cdot 10^{-3}$ | $5.293 \cdot 10^{-2}$ | $2.38 \cdot 10^{-1}$ | $2.30 \cdot 10^{-1}$ |

**Table 3.** LDV locations and statistical properties of surface elevation for Case 6 runs analysed

| Run | Measurement level $z$ (m) | Statistical properties of surface elevation | | | |
|---|---|---|---|---|---|
| | | Mean value (m) | Standard deviation (m) | Skewness | Kurtosis −3 |
| 32 | 0.20 | $-1.06 \cdot 10^{-3}$ | $6.552 \cdot 10^{-2}$ | $2.68 \cdot 10^{-1}$ | $0.95 \cdot 10^{-1}$ |
| 29 | 0.15 | $-1.17 \cdot 10^{-3}$ | $6.498 \cdot 10^{-2}$ | $2.68 \cdot 10^{-1}$ | $1.32 \cdot 10^{-1}$ |
| 19 | 0.10 | $-1.92 \cdot 10^{-3}$ | $6.383 \cdot 10^{-2}$ | $2.55 \cdot 10^{-1}$ | $1.39 \cdot 10^{-1}$ |
| 16 | 0.05 | $-1.57 \cdot 10^{-3}$ | $6.444 \cdot 10^{-2}$ | $2.62 \cdot 10^{-1}$ | $1.27 \cdot 10^{-1}$ |
| 11 | 0.00 | $-1.74 \cdot 10^{-3}$ | $6.404 \cdot 10^{-2}$ | $2.59 \cdot 10^{-1}$ | $1.61 \cdot 10^{-1}$ |
| 6 | −0.10 | $-2.21 \cdot 10^{-3}$ | $6.390 \cdot 10^{-2}$ | $2.62 \cdot 10^{-1}$ | $1.60 \cdot 10^{-1}$ |
| 7 | −0.15 | $-1.64 \cdot 10^{-3}$ | $6.339 \cdot 10^{-2}$ | $2.56 \cdot 10^{-1}$ | $1.46 \cdot 10^{-1}$ |
| 14 | −0.20 | $-1.41 \cdot 10^{-3}$ | $6.847 \cdot 10^{-2}$ | $3.10 \cdot 10^{-1}$ | $0.88 \cdot 10^{-1}$ |
| 22 | −0.25 | $-1.50 \cdot 10^{-3}$ | $6.850 \cdot 10^{-2}$ | $3.00 \cdot 10^{-1}$ | $0.75 \cdot 10^{-1}$ |
| 24 | −0.50 | $-4.46 \cdot 10^{-3}$ | $6.771 \cdot 10^{-2}$ | $2.86 \cdot 10^{-1}$ | $0.76 \cdot 10^{-1}$ |
| 28 | −0.76 | $-0.84 \cdot 10^{-3}$ | $6.381 \cdot 10^{-2}$ | $2.60 \cdot 10^{-1}$ | $1.16 \cdot 10^{-1}$ |
| 26 | −1.00 | $-2.69 \cdot 10^{-3}$ | $6.376 \cdot 10^{-2}$ | $2.65 \cdot 10^{-1}$ | $1.26 \cdot 10^{-1}$ |
| 39 | −1.105 | $-1.40 \cdot 10^{-3}$ | $6.221 \cdot 10^{-2}$ | $2.59 \cdot 10^{-1}$ | $1.66 \cdot 10^{-1}$ |

velocity are given for two elevations. In Figures 8 and 9 as well as 16 and 17 theoretical values of the magnitude of the transfer functions $|T_{\zeta u}|$ and $|T_{\zeta w}|$ are also indicated. They are derived from linear wave theory according to the following expressions:

$$|T_{\zeta u}(\omega)| = \omega \frac{\operatorname{ch} k(z+h)}{\operatorname{sh} kh}, \quad |T_{\zeta w}(\omega)| = \omega \frac{\operatorname{sh} k(z+h)}{\operatorname{sh} kh}, \tag{5}$$

where the wave number $k$ is related to $\omega$ by the dispersion relation:

$$\omega^2(k) = gk \operatorname{th} kh, \tag{6}$$

in which $g$ is the acceleration due to gravity.

In the vicinity of mean water level, lower spectral values for velocities were obtained with increasing $z$-level. This is contrary to expectation of the linear random wave theory when the emergence effect is not taken into account. Moving along vertical axis upwards, the autospectra for $\bar{u}$ and $\bar{w}$ possess a wider bandwidth (see Figures 6, 7 and 14, 15). Moreover, second and third peaks at about $2\omega_p$ and $3\omega_p$ frequencies appear.

The conformity between theoretical (according to linear theory) and observed values of transfer function magnitude is good up to frequencies near twice the primary peak frequency for measurements at low elevations. For higher elevations, however, the linear wave theory without taking the emergence effect into account, gives larger values at all frequencies (see Figures 8, 9 and 16, 17). The degree of over-estimation increases with elevation.

The $\pi$ rads shift can be noticed at frequencies of about half of the primary peak value for the transfer function phase (Figures 10, 11 and 18, 19). It is also noted that for elevation measurements high above the mean water level, $\pi/2$ rads phase shift between surface elevation and vertical velocity is lost, even close to the peak of the wave spectrum (see Figures 11 b and 19 b).

Finally, the coherence functions between the surface elevation $\zeta$ and particle velocities (see Figures 12, 13 and 20, 21) should be examined. The values of coherence at frequencies from half up to twice the value of the primary peak frequency are about 1 for points continuously submerged. Moving further up they fall down being 1 only close to the peak frequency at elevation $z = 0.10$ m. Since the values of the coherence function may be viewed as a measure of the linearity of a system in the absence of noise, it is evident that for points located deeply below the mean water level, linear random wave theory is satisfactory for frequencies up to twice the primary peak frequency. However, in the vicinity of the mean water level the linear relation between surface elevation and velocities becomes invalid. In this region the emergence effect has to be taken into account, when evaluating the stochastic characteristics of the particle kinematics.

## 4. Comparison of Theoretical and Observed Probability Distributions of Velocities

In order to calculate the probability density function and statistical moments for the velocities, the linear part of the spectral density should be known. In the second-order approximation it can be assumed (Appendix A in Part 1) that

$$F(\mathbf{k}) \simeq F^{(1)}(\mathbf{k}). \tag{7}$$

This means that the observed spectrum is identified by its linear part. Moreover, a case when all spectral components propagate in one direction only is considered. In the numerical integration the energy contained in the frequency interval $\omega > 3\omega_p$ was neglected, i.e. an upper frequency cut-off was applied. Thus the frequency spectrum was taken as

$$\tilde{S}(\omega) = S(\omega)\,\mathcal{H}(3\omega_p - \omega), \tag{8}$$

in which $S(\omega)$ is measured spectral density of free elevation ($S_{\zeta\zeta}(\omega)$ in the previous section).

As the wave is unidirectional, the formulae describing the moments for processes $\zeta$, $\mathbf{u}$ (Part 1) become much simpler. Using a polar coordinate system $(k, \theta)$ in the $\mathbf{k}$-vector plane, a directional spectrum $\hat{F}(\omega, \theta)$ is introduced satisfying the relation (154)*. Since the wave is unidirectional, integration over $\theta$ may be carried out immediately, giving

$$S(\omega) = \int_{-\pi}^{\pi} \hat{F}(\omega, \theta)\, d\theta. \tag{9}$$

In the simplified expressions for unidirectional seas corresponding to equations (86)* to (88)* and (120)* to (124)* only the frequency spectrum appears. In the numerical calculations the integrands are expressed in terms of frequencies $\omega$ and $\omega'$ by the dispersion relation (6). Relevant formulae for these simplified expresions are presented in Appendix A.

Double integrals $\int_\omega \int_{\omega'} \ldots \tilde{S}(\omega)\tilde{S}(\omega')\, d\omega\, d\omega'$ were calculated using a highly efficient iterative procedure described in the previous section.

Figures 22 and 23 show the observed probability distribution for horizontal and vertical velocities for the different elevations for Case 5. Figures 24 and 25 show the distributions of the same quantities for Case 6. In the same figures the continuous parts of the density function given in equation (48)* are presented leaving out the discrete part. The observed probabiblity distribution for time series $\bar{u}_i$ and $\bar{w}_i$ are estimated and then scaled in the same manner as the surface elevation $\zeta_i$ (see equation (4)). The only difference is that the modified velocity values given in equation (1) which are equal to zero and correspond to $\zeta_i < z$, are not counted in the appropriate bin. For the elevations $z = -0.05$ m and $z =$

0.00 m the theoretical results (when the emergence effect is taken into account) are in close agreement with the observed values. When the measurement point of the LDV station is above the mean water level the agreement is slightly better when the non-linearity of the wave motion is included, i.e. formula (32)* compares better with the experimental data. For the lower position of the LDV station the differences due to weak second-order non-linearities are marginal. However, the emergence effect is still important for elevations $z > -3\sigma_\zeta$. In Figures 22, 23 and 24, 25 the Gaussian probability density function is marked for comparison.

The density functions for horizontal velocity component are generally skewed while those for vertical velocity are non-skewed.

Figures 26 and 28 show the variation of the mean value and standard deviation along the $z$-axis for horizontal and vertical velocity, respectively. It can be noted that differences between theoretical values due to second-order non-linear effects (equations (45)* and (46)*) and without these effects (equations (49)* and (50)*) are negligible. Only slightly better agreement for the standard deviation of horizontal velocity in the second order approximation can be noticed. The observed values show a high degree of agreement with theoretical values obtained with the emergence effect taken into account and also compare well with the findings of Anastasiou *et al.* (1982a, b). However, for the mean value of the horizontal velocity, the observed values do not compare well with those obtained theoretically. It seems that the existence of the return current in a confined wave flume could be an explanation of that departure. The emergence effect "produces" a positive mean value of the horizontal velocity (an apparent current) in the vicinity of the mean water level. This current, directed in the positive $x$-axis, has to be balanced by the return current. In this way the measured values of the horizontal component of the particle velocity will be influenced by the back flow in the wave tank. In fact it should be stated that the theory presented in Part 1 in the case of horizontal velocities can not be verified by the data taken from a closed wave flume. These theoretical results may be valid only for waves in the open sea. Note that we are not able to introduce the simplest solution suggested for the return flow problem, i.e. assumption of a uniform distribution. We operate in the domain $z \in [-h, \infty)$ and such an assumption would not have made sense.

However, we can rephrase the problem. If we believe that the results obtained in Part 1 are correct, then we can suggest that the difference between the predicted and the measured values gives an estimate of the return current in the wave flume! In Figure 27 the measured mean horizontal velocities are marked with stars for wave cases I18 and I24. The dashed line presents the theoretical mean value of the horizontal velocities with emergence effect taken into account, according to equation (49)*. Open circles show the estimated values of the return flow as described above. It should be emphasised that the only "true" objects in that figure are points for the measured and estimated velocities of the mean horizontal velocity and the estimated return flow, respectively, as well as the curve

for theoretical mean horizontal velocity. The solid lines for the measured mean velocity and the estimated return flow should be treated as "intuitive guesses" of the appropriate vertical mean velocity profiles. They were obtained by use of cubic spline interpolation.

The interpolated profiles as well as the theoretical values for the positive mean value of the horizontal velocity were used to estimate the measured positive and negative total flows $q_m^+$, $q_m^-$, respectively, and the predicted positive total mean flow $q^+$, induced by the waves, and the estimated return flow $q^-$. Let us denote

$$\left.\begin{aligned} \chi_m^{\pm} &= \frac{\Delta q_m}{|q_m^{\pm}|}, \quad \chi_m = \frac{\chi_m^+ + \chi_m^-}{2} \\ \chi^{\pm} &= \frac{\Delta q}{|q^{\pm}|}, \quad \chi = \frac{\chi^+ + \chi^-}{2} \end{aligned}\right\}, \tag{10}$$

where $\Delta q_m = q_m^+ + q_m^-$ and $\Delta q = q^+ + q^-$. The values $q^+$ obtained from theoretical formula (152)* for wave cases I18 and I24 are presented in Table 4. It denotes the positive total mean flux calculated by numerical integration with the spectrum $S(\omega)$ estimated from the time series $\zeta$. Table 4 furthermore shows the quantites $\Delta q$, $\Delta q_m$ obtained from numerical computations together with the coefficients $\chi$ and $\chi_m$. Note that the above values (except the values for $q^+$ which are calculated from the theoretical expression) are influenced by the authors' "intuitive guess" expressed in artificial lines and that they should be treated as rough estimation. Nevertheless, the numerical results obtained for $\chi$s in (10) of the order of 5% (see Table 4) indicate that the constraint of zero net mass flow seems to be fulfilled.

**Table 4.** Numering results for Wave Cases 5 and 6

| Wave Case | $q^+$ ($m^2s^{-1}$) | $\Delta q$ ($m^2s^{-1}$) | $\chi$ | $q_m^+$ ($m^2s^{-1}$) | $\Delta q_m$ ($m^2s^{-1}$) | $\chi_m$ |
|---|---|---|---|---|---|---|
| 5 | 0.0115 | $1.61 \cdot 10^{-4}$ | 0.014 | 0.0082 | $3.76 \cdot 10^{-4}$ | 0.047 |
| 6 | 0.0145 | $-9.18 \cdot 10^{-4}$ | 0.061 | 0.0096 | $-6.38 \cdot 10^{-4}$ | 0.064 |

Zero mean value of vertical velocity for all elevations follows from formulas (45)*, (123)* and (130)*. This agreed very well with observations, cf. Figure 28.

Figure 29 shows the skewness of the horizontal velocity calculated with the help of (124)* and (125)* (when weak non-linearities are taken into account). These values appear to be slightly negative, which is in close agreement with measured skewness at the elevations deeply below the mean water level where the emergence effect is not important. Anastasiou *et al.* (1982b) also noted the negative skewness values for horizontal velocity. Due to the emergence effect the skewness becomes positive close to the mean water level, cf. Figure 29. The theoretical predictions for

the skewness of the horizontal velocity with emergence effect taken into account (for cases with and without second-order non-linear effects) are also presented in Figure 29. They were obtained by numerical integration of the probability density (32)* and compare well with observed skewness.

The skewness of the vertical velocity, for points below the mean water level, is zero in accordance with equation (128)*. This is confirmed in Figure 29 where the calculated skewness of the measured vertical velocities is marked with open circles.

## 5. Conclusions

Following the development of the theoretical predictions, wave surface and wave kinematics measurements are analysed, with particular emphasis on the near surface kinematics. For wave cases I18 and I24 generated from an almost linear wave surface spectrum, it is demonstrated that non-linearities play a marginal effect on the measured kinematics and that non-Gaussian parts of the statistics of wave kinematics mainly relate to the emergence effects. For a sea state generated from a more strongly non-linear surface spectrum it is, however, expected that the effects on the kinematics from the surface non-linearities would have been significant.

Excellent correlation between the statistical measurements and theoretical results presented in Part 1 has been found, thus demonstrating the usefulness of this theoretical development. The only difference found between predictions and measurements being that for the mean value of the horizontal velocity near the free surface.

The theoretical results of this study, when applied to horizontal velocities, are valid only in open water. It follows that these results can not be directly verified with measurements taken in a wave tank. However, if we *postulate* that these theoretical results are correct, then we can suggest that the difference between the predicted and the measured values gives an estimate of the return current in the wave flume. The postulate that the formulae obtained in this paper are correct is supported by two factors:

1. That the expression for the total mean flux in approximation is known and well-interpreted, as was mentioned above.
2. That the approach for estimating such stochastic properties of random water wave kinematics, that are not influenced by the return flow (i.e. mean value of the vertical velocity and standard deviation for both horizontal and vertical velocity components) agree very well with the measurements in the wave flume.

Experimentalists do not normally study kinematics in the free surface zone. This is mainly due to technical difficulties associated with data collection in this

zone. The measurements have usually been stopped at an elevation where interesting phenomenon appear. The first measurements of wave kinematics near the mean water level (up to one standard deviation of the surface elevation above that level) were as such reported by Anastasiou *et al.* (1982a, b). The data set which has been examined in this paper is, however, unique in the sense that it has been possible to examine the variation of the velocity along the vertical axis up to a level of about four standard deviations of the surface elevation and down to the bottom of the wave flume with measurements spaced close enough to prepare the profiles for the statistical properties of the velocities.

Reviewing the I18 and I24 wave cases, currents in opposite directions to each other have been noticed. While the emergence effect explains the existence of the current in the direction of wave advance, the nature of the return current which appears just below the mean water level is still unresolved (at least for irregular waves). To answer the question why this layer is "preferred" by the backflowing water, it may be necessary to take into account the viscosity of the fluid in the near boundary regions and the vorticity which diffuses and convects throughout the wave flume. Energy dissipation and the turbulence in the free surface zone may also be important factors which influence the shape of the mean horizontal velocity profile. For a complete study of the problem of the return flow in a flume, the full three-dimensional geometry and details of wave absorption need to be considered.

Further work will concentrate on evaluation of other data series to examine the influence of wave steepness on wave kinematics and on further prediction of return flow in a wave flume (see also Gudmestad and Haver 1993).

## Acknowledgements

The authors would like to thank Dr. J. Skjelbreia and Prof. A. Tørum for their efforts providing the unique data material which has made verification of the theoretical prediction possible. This data collection was funded by the Norwegian Council for Scientific and Industrial Research, Statoil, Amoco, Conoco, Exxon and Mobil.

## References

Anastasiou K., Tickell R. G., Chaplin J. R. (1982a): Measurements of particle velocities in laboratory-scale random waves, *Coastal Engineering*, Vol. 6, pp. 233–254.

Anastasiou K., Tickell R. G., Chaplin J. R. (1982b): The non-linear properties of random wave kinematics, *BOSS 82—Proceedings of the Third International Conference on the Behaviour of Offshore Structures*, Vol. 1, pp. 493–515.

Cieślikiewicz W., Gudmestad O. T. (1994): Random water wave kinematics. Part 1. Theory, *Archives of Hydro-Engineering and Environmental Mechanics*, Vol. 41, No. 1.

Gudmestad O. T., Haver S. (1993): Uncertainties in prediction of wave kinematics in irregular waves, *SUT Conf. Environmental forces and wave kinematics*, London.

Ochi M. K., Wang W. C. (1984): Non-gaussian characteristics of coastal waves, *Proc. 19th Coastal Eng. Conf.*, Vol. 1, pp. 516–531.

Oppenheim A. V., Schafer R. W. (1975): *Digital Signal Processing*, Englewood Cliffs, N. J., Prentice Hall.

Skjelbreia J., Tørum A., Berek E., Gudmestad O. T., Heideman J., Spidsøe N. (1989): Laboratory measurements of regular and irregular wave kinematics, *E&P Forum Workshop on Wave and Current Kinematics and Loading IFP*, Rueil Malmaison, France, pp. 45–66.

Skjelbreia J. E., Berek E., Bolen Z. K., Gudmestad O. T., Heideman J. C., Ohmart R. D., Spidsøe N., Tørum A. (1991): Wave kinematics in irregular waves, *Proc. 10th Intern. Conf. on Offshore Mechanics and Arctic Eng.*, Stavanger, Norway, pp. 223–228.

Zelt J. A., Skjelbreia J. E. (1992): Estimating incident and reflected wave fields using an arbitrary number of wave gauges, *Proc. 23th Coastal Eng. Conf.*, Venice, Italy.

## Appendix A

In this appendix the formulae for parameters of the probability distribution for velocities in the one-directional case will be given. In the notation the following equivalences are used

$$\tilde{k} \equiv \frac{\omega^2}{g} \quad \tilde{k}' \equiv \frac{\omega'^2}{g}, \tag{A1}$$

and for a given angular frequency $\omega$, the wave number $k$ is calculated by the dispersion relation (6). We leave the equation numbers as in Part 1 marking them additionally with primes. The relevant formulae are as follows:

$$m_{10} = \frac{1}{2} \int_{\omega} \tilde{k} \left(1 - \frac{k^2}{\tilde{k}^2}\right) \tilde{S}(\omega)\, d\omega, \tag{86'}$$

$$\mu_{20} = \int_{\omega} \tilde{S}(\omega)\, d\omega, \tag{87'}$$

$$\mu_{30} = \int_{\omega} \int_{\omega'} K_{30}(\omega, \omega')\, \tilde{S}(\omega)\, \tilde{S}(\omega')\, d\omega\, d\omega', \tag{88'}$$

$$K_{30}(\omega, \omega') = \frac{3}{\sqrt{\tilde{k}\tilde{k}'}} B(\omega, \omega'), \tag{89'}$$

$$B(\omega, \omega') = B^{-}(\omega, \omega') + B^{+}(\omega, \omega') - kk' + (\tilde{k} + \tilde{k}')\sqrt{\tilde{k}\tilde{k}'}, \tag{90'}$$

$$B^{\pm}(\omega, \omega') = \frac{\left(\sqrt{\tilde{k}} \pm \sqrt{\tilde{k}'}\right)^2 \left(kk' \mp \tilde{k}\tilde{k}'\right) + \left(\sqrt{\tilde{k}} \pm \sqrt{\tilde{k}'}\right)\left(\sqrt{\tilde{k}'} R \pm \sqrt{\tilde{k}} R'\right)}{\left(\sqrt{\tilde{k}} \pm \sqrt{\tilde{k}'}\right)^2 - |k \pm k'| \operatorname{th} |k \pm k'| h}, \tag{91'}$$

$$R = \frac{1}{2}(k^2 - \tilde{k}^2) \quad R' = \frac{1}{2}(k'^2 - \tilde{k}'^2), \tag{92'}$$

$$m_{01}^{u_\nu} = 0 \qquad \text{for} \quad \nu = 1, 3, \tag{119'}$$

$$\mu_{02}^{u_1} = g \int_\omega \frac{k^2}{\tilde{k}} \frac{\operatorname{ch} 2k(z+h) + 1}{\operatorname{ch} 2kh + 1} \tilde{S}(\omega)\, d\omega, \tag{120'}$$

$$\mu_{02}^{u_3} = g \int_\omega \tilde{k} \frac{\operatorname{ch} 2k(z+h) - 1}{\operatorname{ch} 2kh - 1} \tilde{S}(\omega)\, d\omega, \tag{121'}$$

$$\mu_{11}^{u_1} = \int_\omega \sqrt{\frac{g}{\tilde{k}}} k \frac{\operatorname{ch} k(z+h)}{\operatorname{ch} kh} \tilde{S}(\omega)\, d\omega, \tag{122'}$$

$$\mu_{11}^{u_3} = 0, \tag{123'}$$

$$\mu_{mn}^{u_\nu} = \int_\omega \int_{\omega'} K_{mn}^{u_\nu}(\omega, \omega'; z) \tilde{S}(\omega)\, \tilde{S}(\omega')\, d\omega\, d\omega', \tag{124'}$$

$$K_{03}^{u_1}(\omega, \omega'; z) = 3g\sqrt{g} \frac{kk'}{\tilde{k}\tilde{k}'} \left[ (k - k')\, C^-(\omega, \omega'; z) + (k + k')\, C^+(\omega, \omega'; z) \right] \frac{\operatorname{ch} k(z+h) \operatorname{ch} k'(z+h)}{\operatorname{ch} kh \operatorname{ch} k'h}, \tag{125'}$$

$$C^\pm(\omega, \omega'; z) = \frac{B^\pm(\omega, \omega')}{\sqrt{\tilde{k}} \pm \sqrt{\tilde{k}'}} \frac{\operatorname{ch} k^\pm(z+h)}{\operatorname{ch} k^\pm h}, \tag{126'}$$

$$k^\pm = |k \pm k'|, \tag{127'}$$

$$K_{03}^{u_3} = 0, \tag{128'}$$

$$K_{21}^{u_1}(\omega, \omega'; z) = \sqrt{\frac{g}{\tilde{k}\tilde{k}'}} \left\{ (k - k')\, C^-(\omega, \omega'; z) + (k + k')\, C^+(\omega, \omega'; z) + \frac{2k'}{\sqrt{\tilde{k}'}} B(\omega, \omega') \frac{\operatorname{ch} k'(z + h)}{\operatorname{ch} k'h} \right\}, \tag{129'}$$

$$K_{21}^{u_3} = 0, \tag{130'}$$

$$K_{12}^{u_1}(\omega, \omega'; z) = \frac{gk'}{\tilde{k}'\sqrt{\tilde{k}}} \frac{\operatorname{ch} k'(z + h)}{\operatorname{ch} k'h} \left\{ \frac{k}{\sqrt{\tilde{k}}} B(\omega, \omega') \frac{\operatorname{ch} k(z + h)}{\operatorname{ch} kh} + 2\left[ (k - k')\, C^-(\omega, \omega'; z) + (k + k')\, C^+(\omega, \omega'; z) \right] \right\}, \tag{131'}$$

$$K_{12}^{u_3}(\omega, \omega'; z) = g \frac{\operatorname{sh} k'(z + h)}{\operatorname{sh} k'h} \left\{ \left[ B^-(\omega, \omega') - B^+(\omega, \omega') - \tilde{k}\tilde{k}' \right] \frac{\operatorname{sh} k(z + h)}{\operatorname{sh} kh} - \frac{2}{\sqrt{\tilde{k}}} \left[ |k - k'| \operatorname{th} |k - k'| h\, D^-(\omega, \omega'; z) - |k + k'| \operatorname{th} |k + k'| h\, D^+(\omega, \omega'; z) \right] \right\}, \tag{132'}$$

$$D^{\pm}(\omega, \omega'; z) = C^{\pm}(\omega, \omega'; z) \frac{\operatorname{ch} k^{\pm}(z + h)}{\operatorname{ch} k^{\pm}h}. \tag{133'}$$

## Appendix B

This appendix contains all figures discussed in this paper.

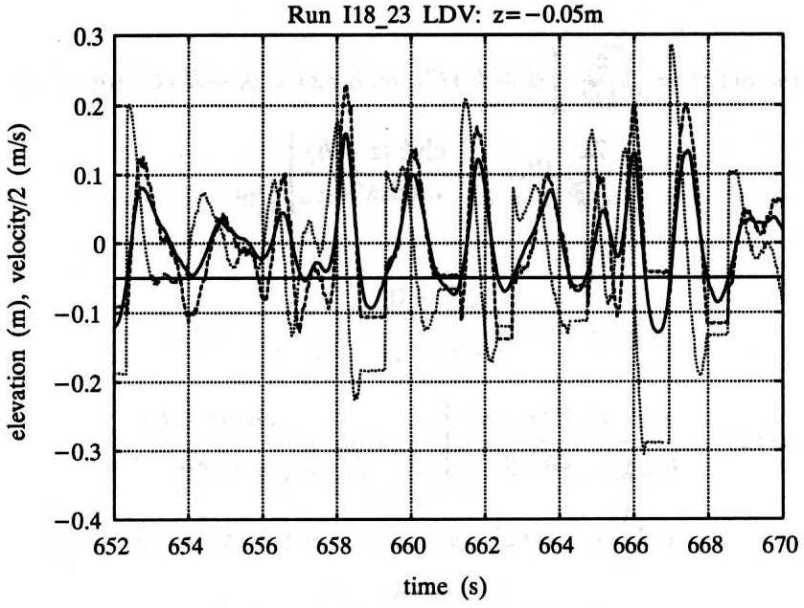


**Fig. 1.** Sample of measured time series: ———— surface elevation, – – – – horizontal velocity, ····· vertical velocity (both velocities are scaled by factor 0.5). Solid, horizontal line indicates the elevation of LDV station; Note that the velocities are without modification

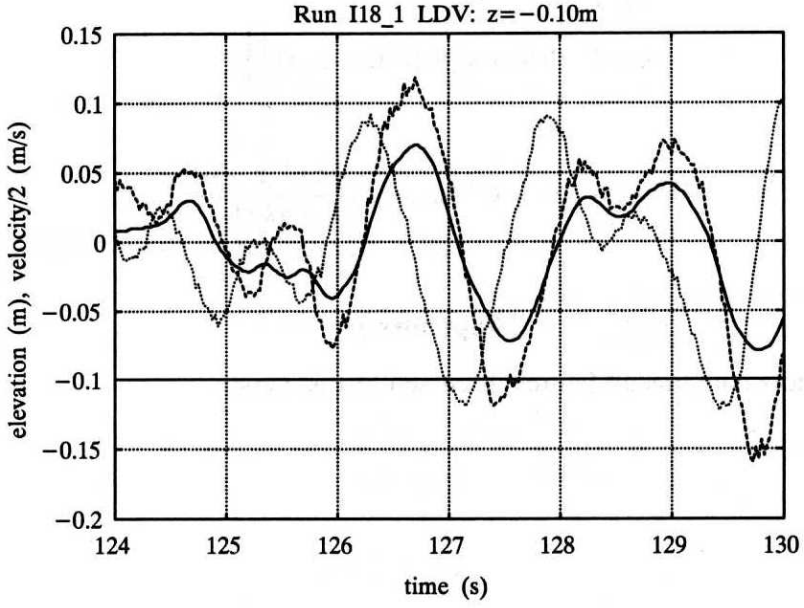


**Fig. 2a.** Examples of measured surface elevation (————) and modified velocities (– – – – horizontal, ····· vertical) for various LDV elevations

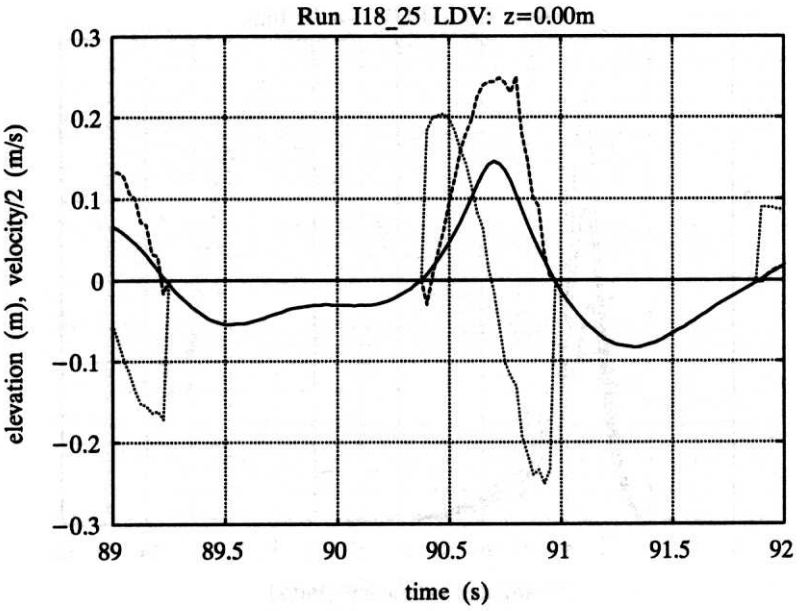


**Fig. 2b.** See Fig. 2a

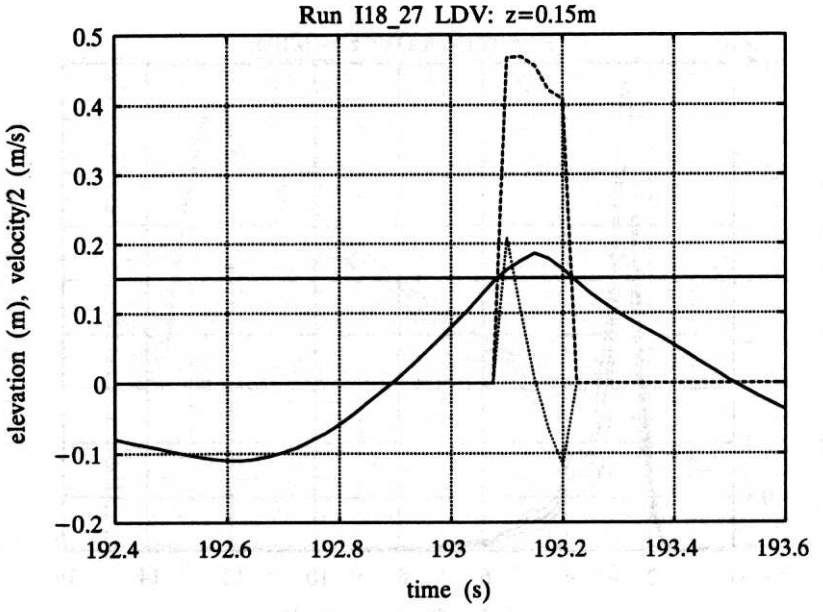


**Fig. 2c.** See Fig. 2a

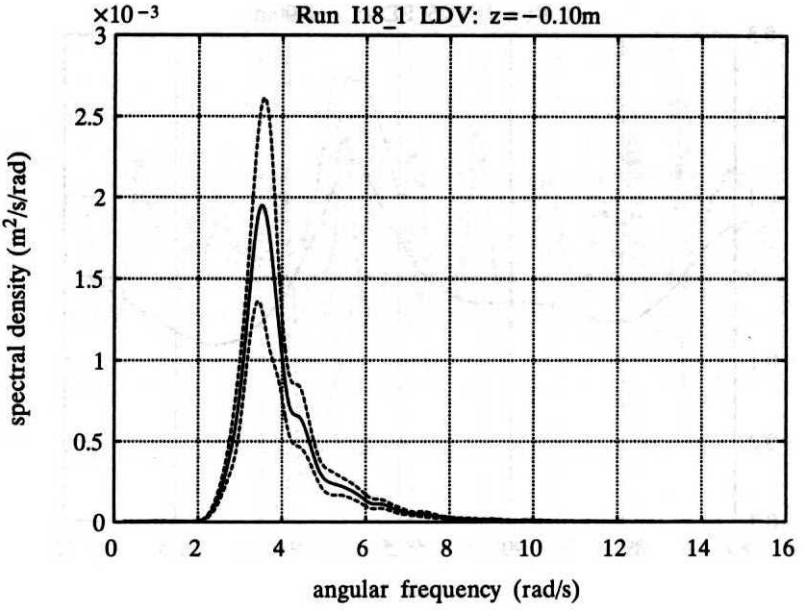


**Fig. 3a.** Power spectrum of free surface elevation for a) Run 1 of case I18, b) Run 6 of case I24; – – – – 95% confidence limits

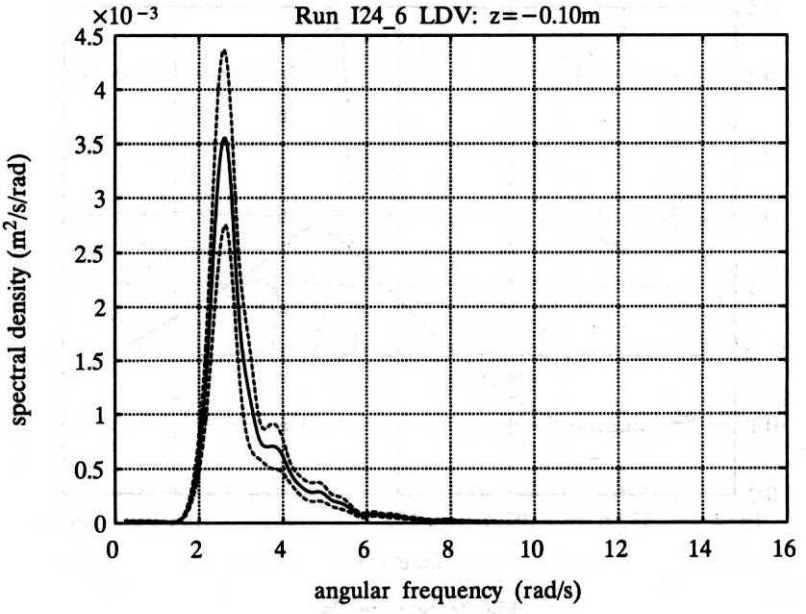


**Fig. 3b.** See Fig. 3a

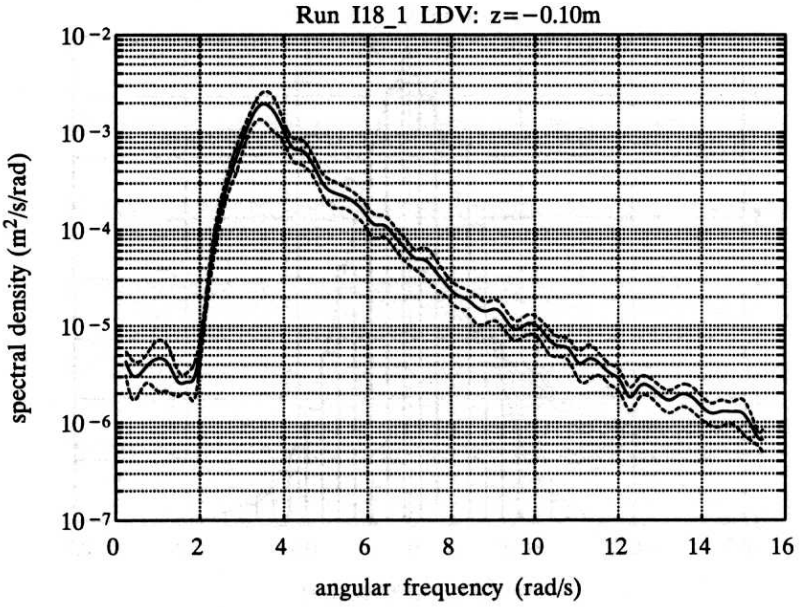


**Fig. 4a.** Power spectrum of free surface elevation in logarithmic scale for a) Run 1 of case I18, b) Run 6 of case I24; – – – – 95% confidence limits

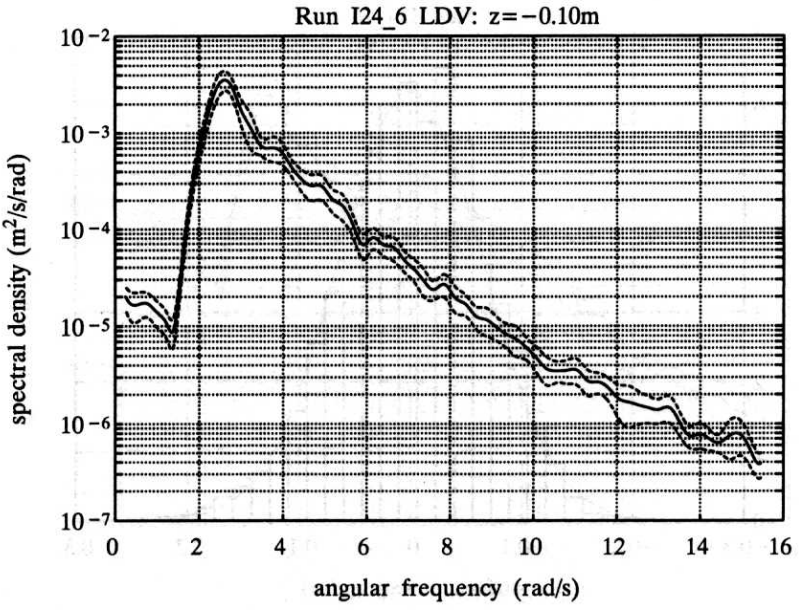


**Fig. 4b.** See Fig. 4a

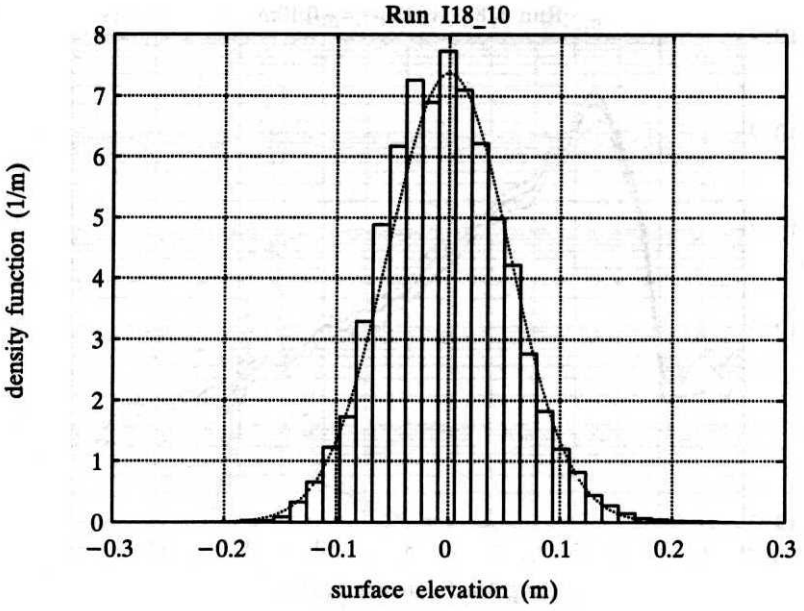


**Fig. 5a.** Comparison of the observed (bar plot) and Gaussian probability distribution (·····) for a) Run 10 of case I18 and b) Run 16 of case I24

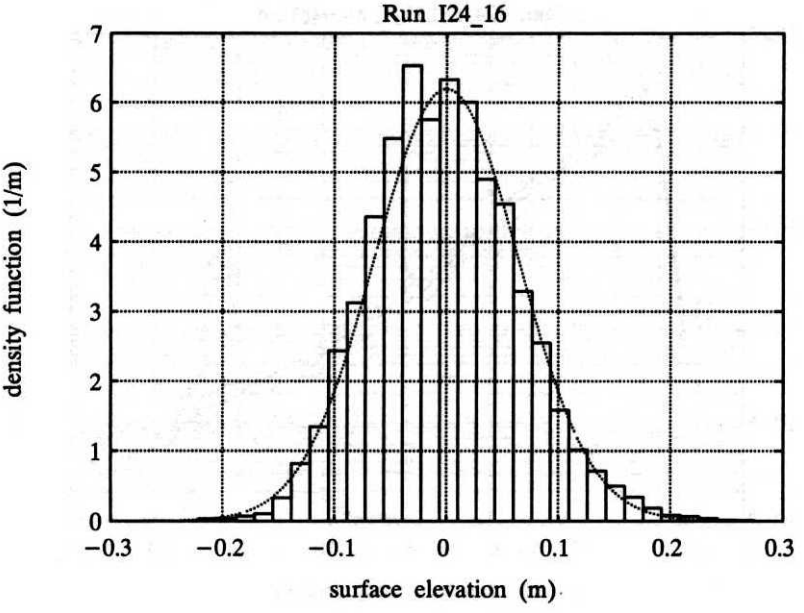


**Fig. 5b.** See Fig. 5a

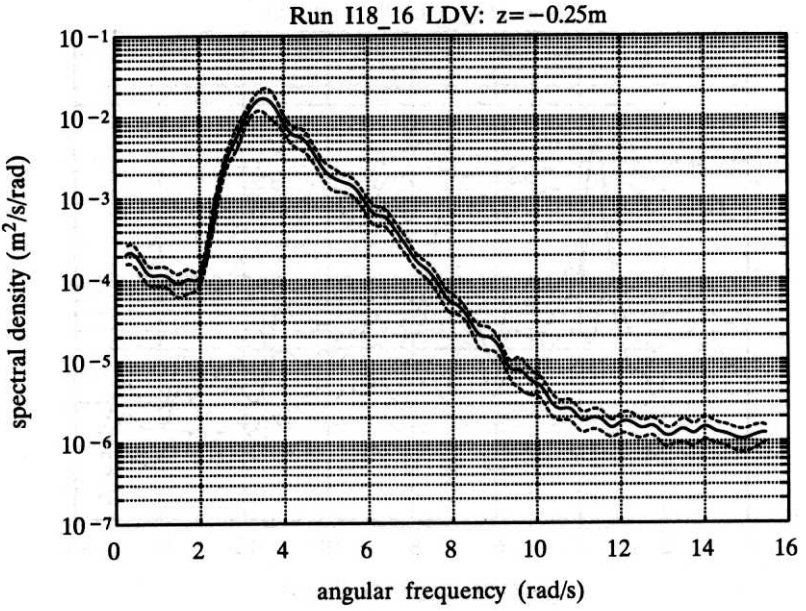


**Fig. 6a.** Spectra of horizontal velocity for various $z$; – – – – 95% confidence limits. Wave case I18

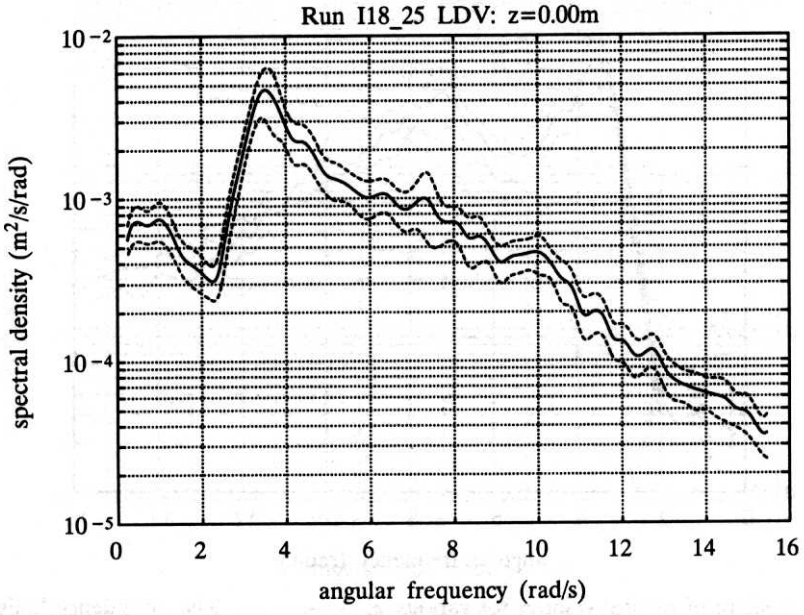


**Fig. 6b.** See Fig. 6a

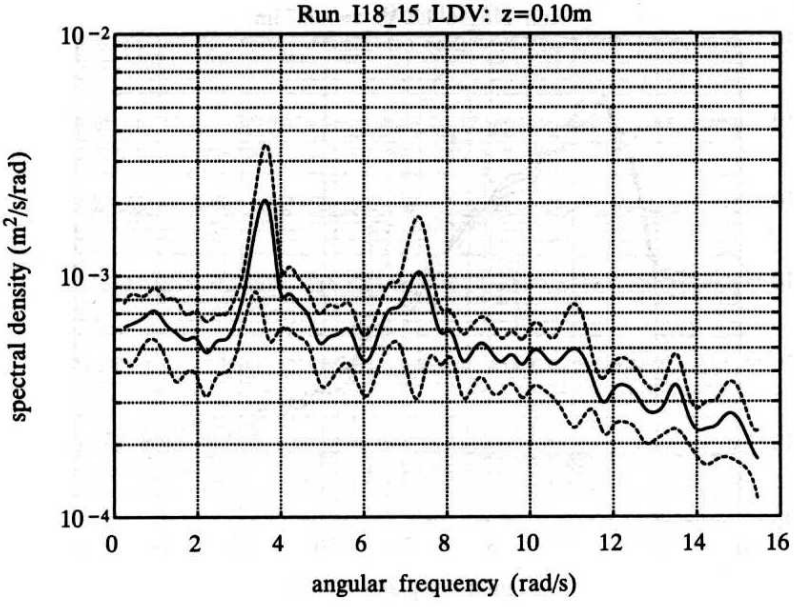


**Fig. 6c.** See Fig. 6a

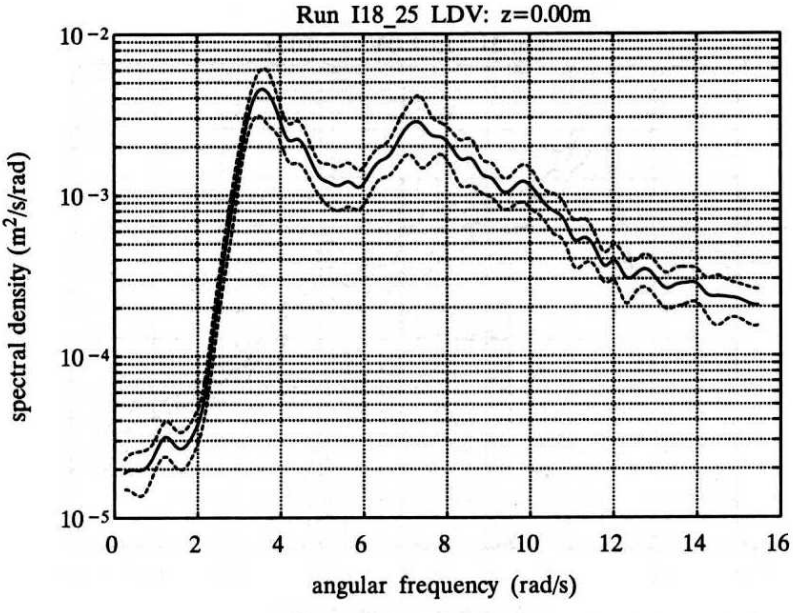


**Fig. 7a.** Spectra of vertical velocity for various $z$; – – – – 95% confidence limits. Wave case I18

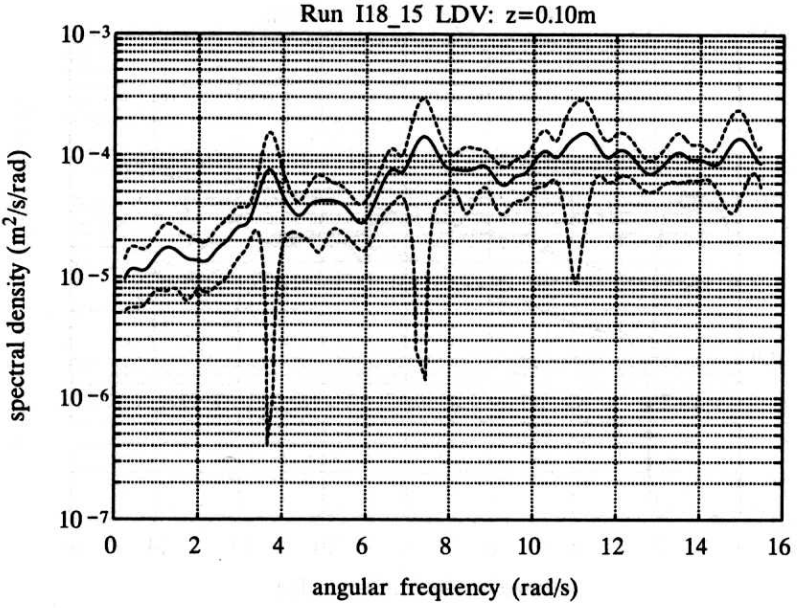


**Fig. 7b.** See Fig. 7a

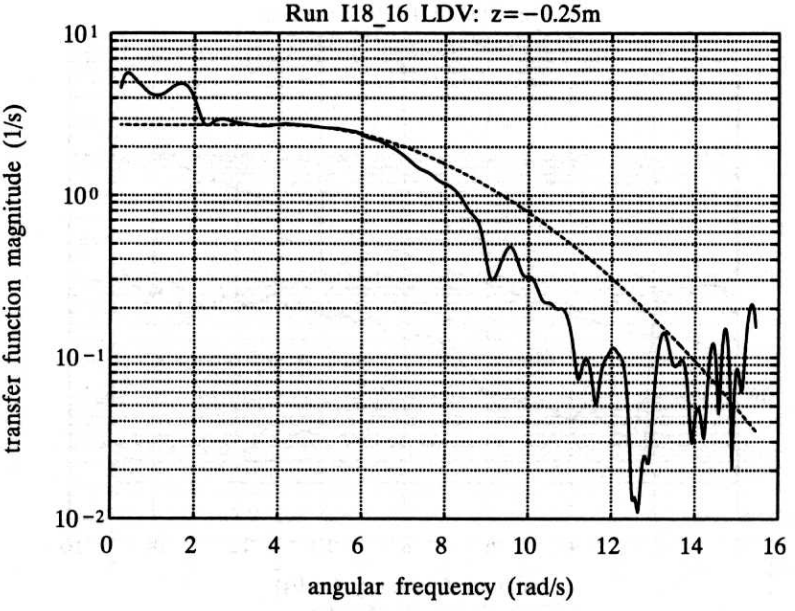


**Fig. 8a.** Magnitude of transfer function between surface elevation and horizontal velocity for various $z$; ———— observed, – – – – according to linear random wave theory. Wave case I18

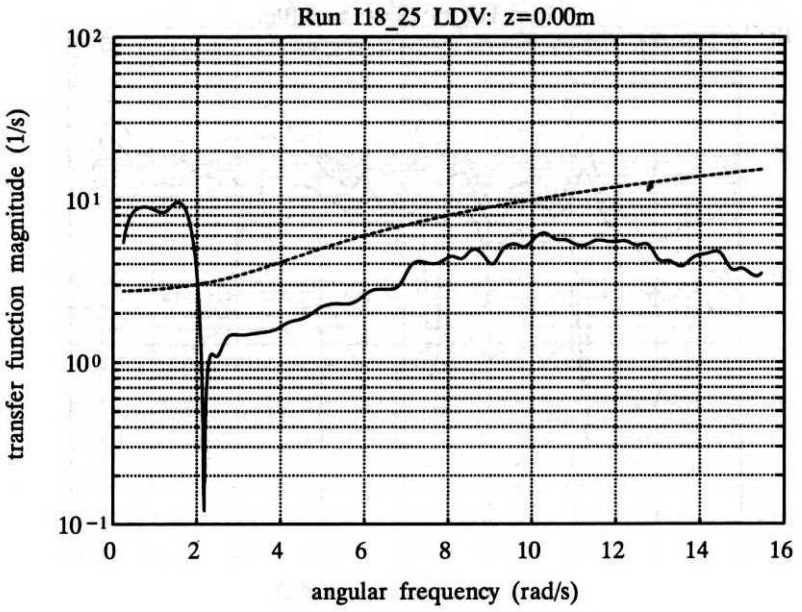


**Fig. 8b.** See Fig. 8a

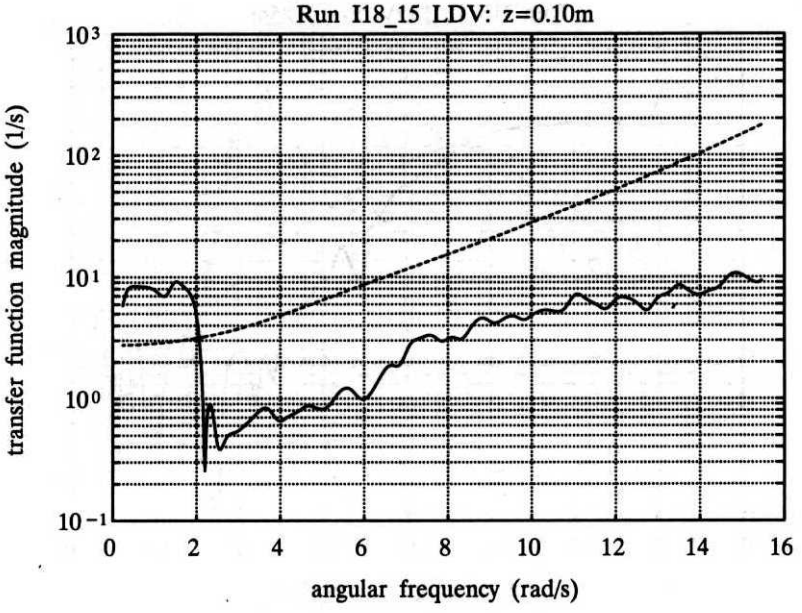


**Fig. 8c.** See Fig. 8a

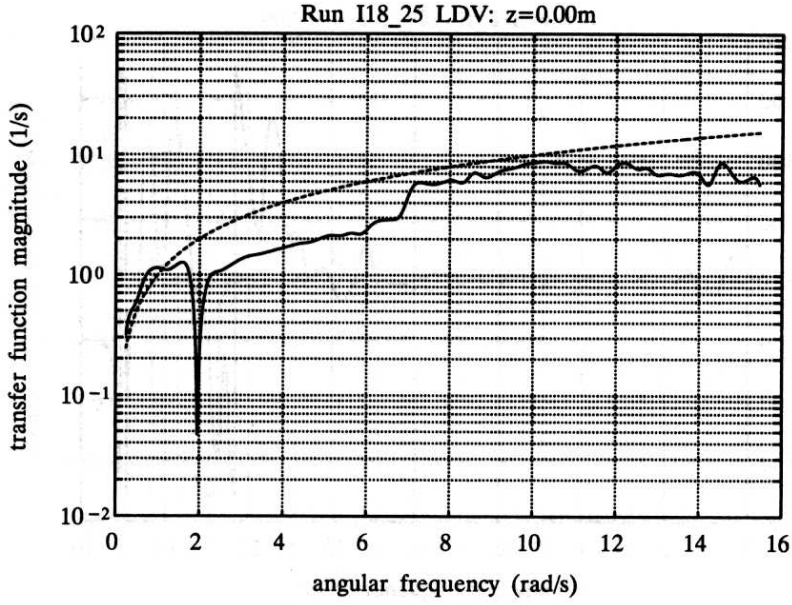


**Fig. 9a.** Magnitude of transfer function between surface elevation and vertical velocity for various $z$; ———— observed, – – – – according to linear random wave theory. Wave case I18

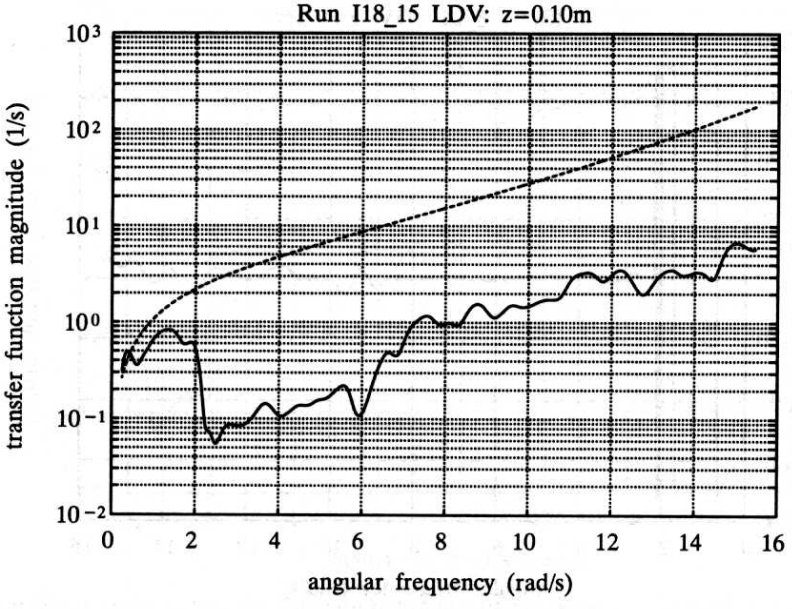


**Fig. 9b.** See Fig. 9a

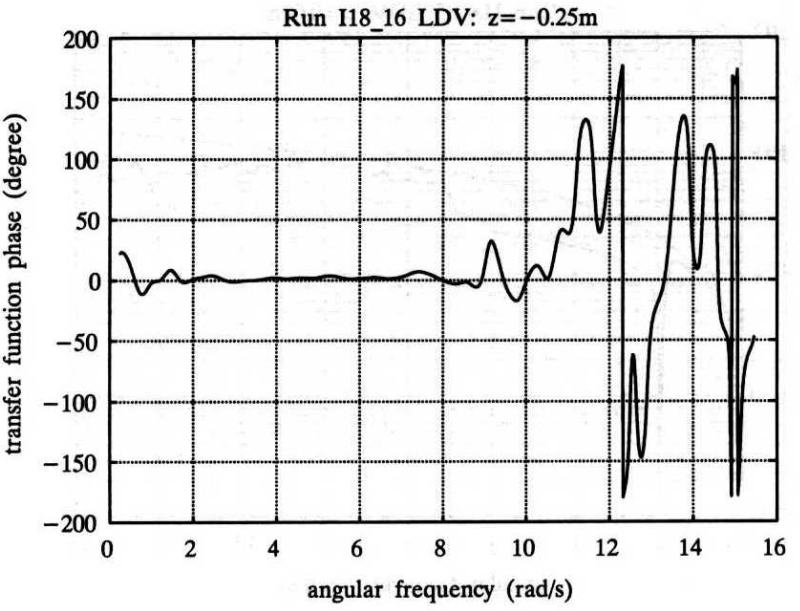


**Fig. 10a.** Phase angle of transfer function between surface elevation and horizontal velocity for various $z$. Wave case I18

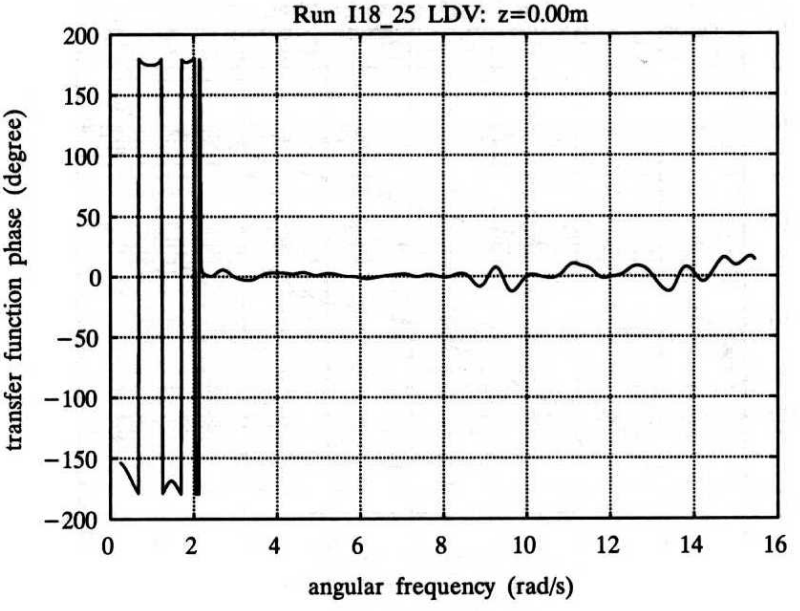


**Fig. 10b.** See Fig. 10a

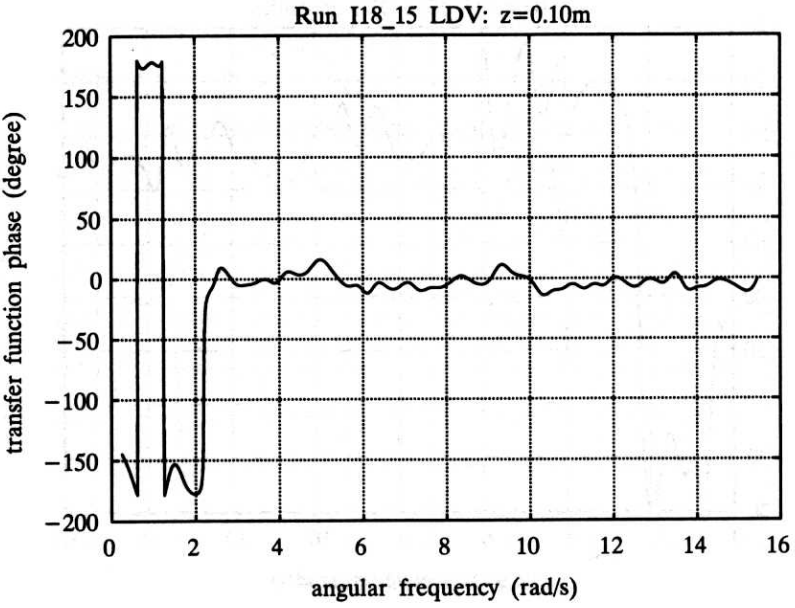


**Fig. 10c.** See Fig. 10a

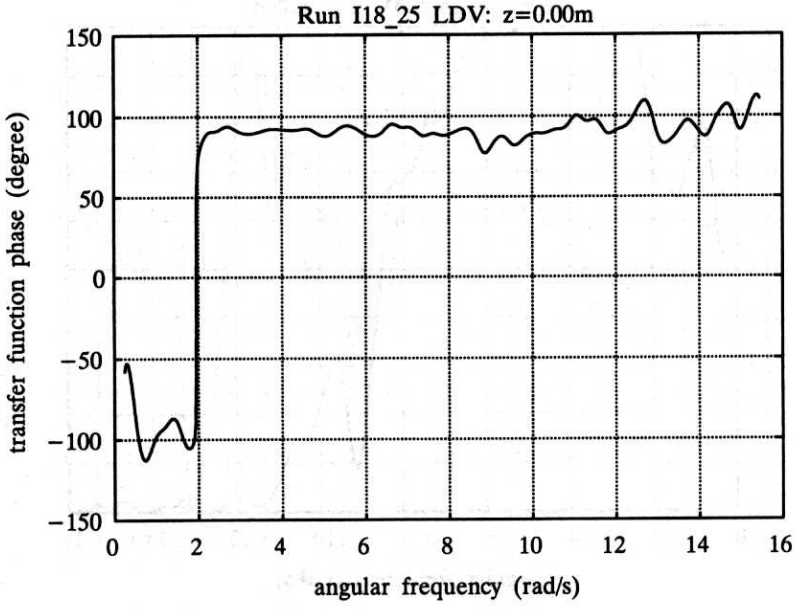


**Fig. 11a.** Phase angle of transfer function between surface elevation and vertical velocity for various $z$. Wave case I18

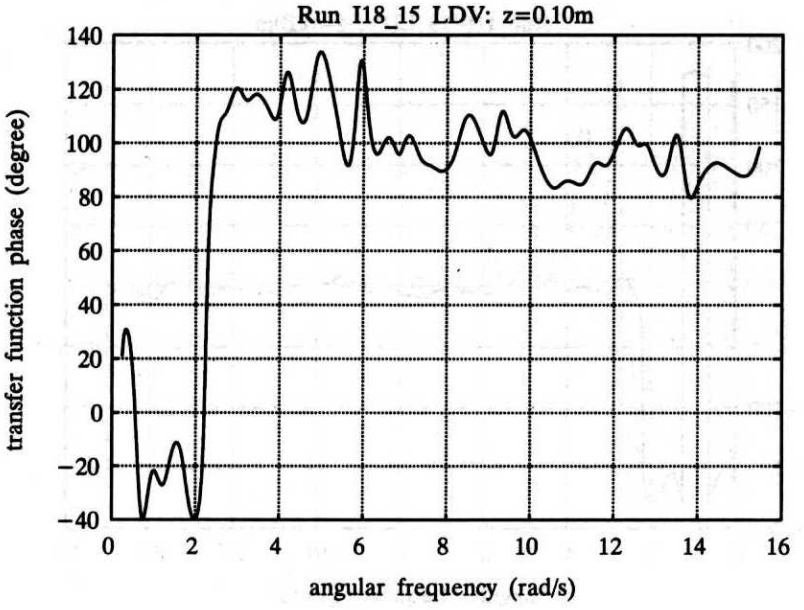


**Fig. 11b.** See Fig. 11a

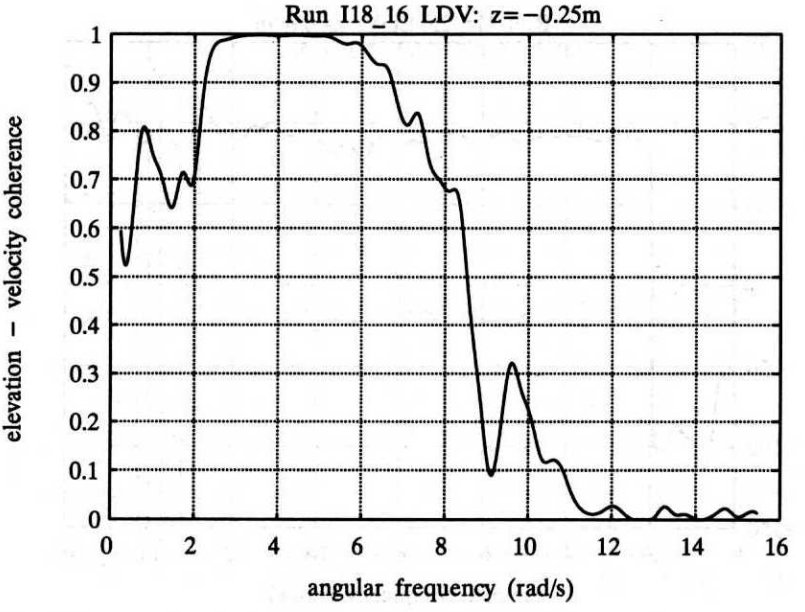


**Fig. 12a.** Coherence function between surface elevation and horizontal velocity for various $z$. Wave case I18

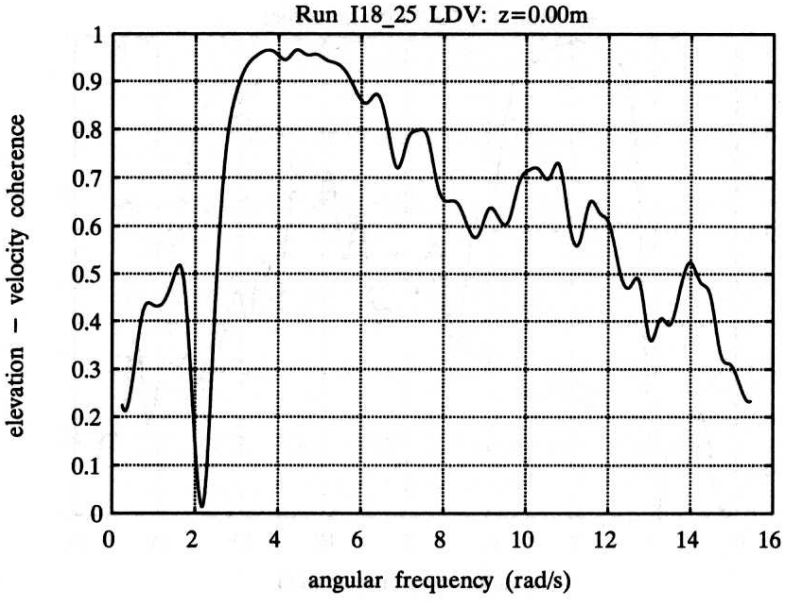


**Fig. 12b.** See Fig. 12a

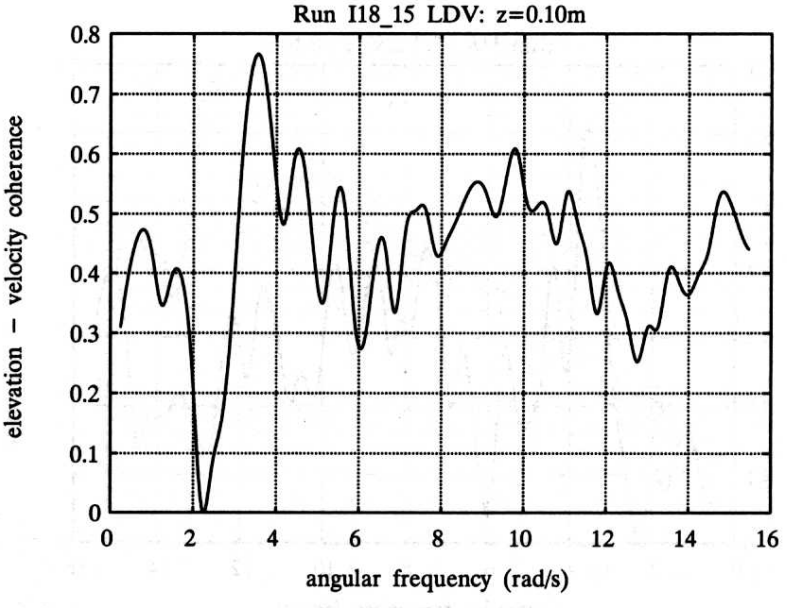


**Fig. 12c.** See Fig. 12a

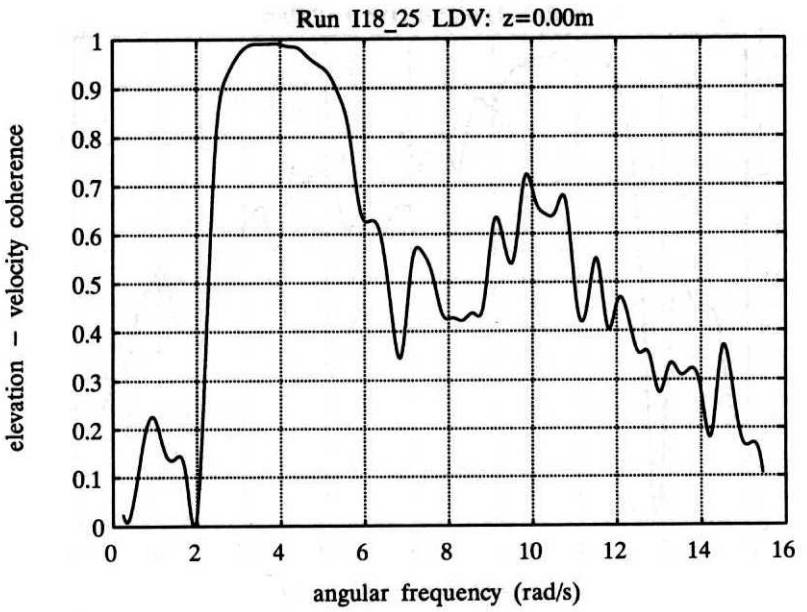


**Fig. 13a.** Coherence function between surface elevation and vertical velocity for various $z$. Wave case I18

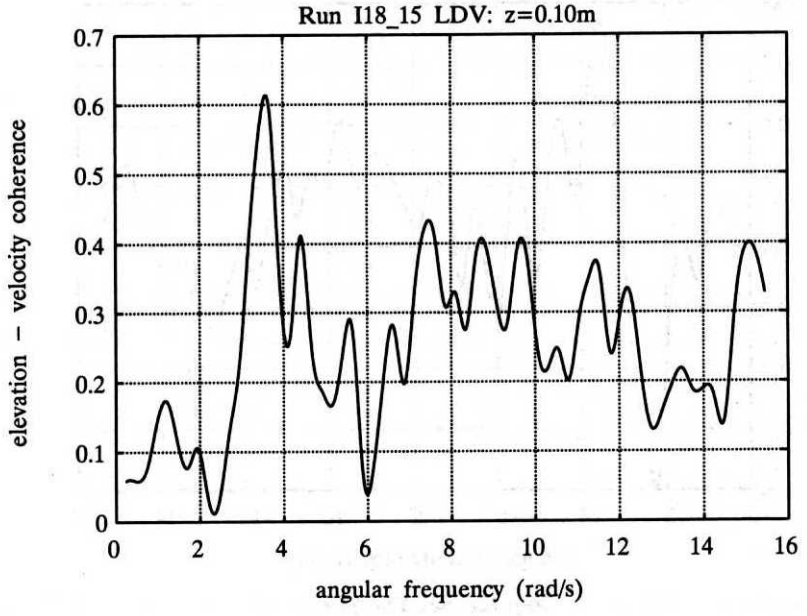


**Fig. 13b.** See Fig. 13a

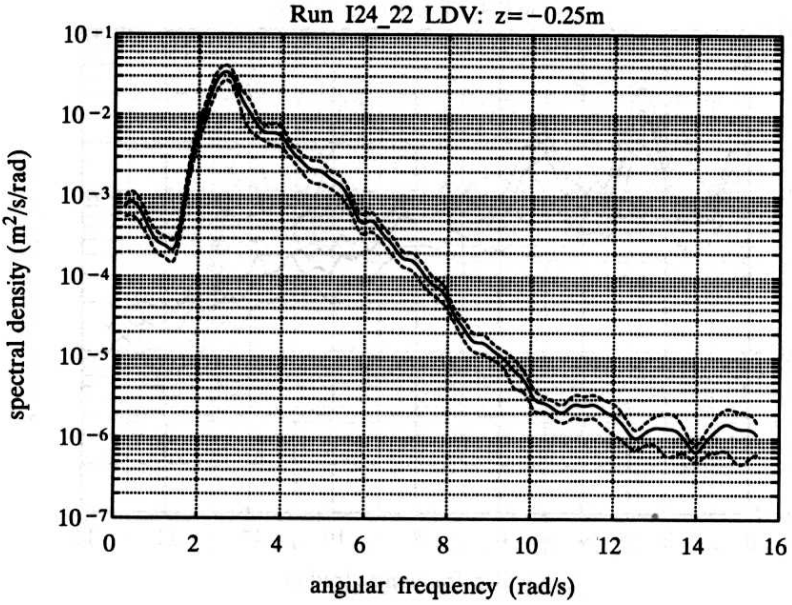


**Fig. 14a.** Spectra of horizontal velocity for various $z$; – – – – 95% confidence limits. Wave case I24

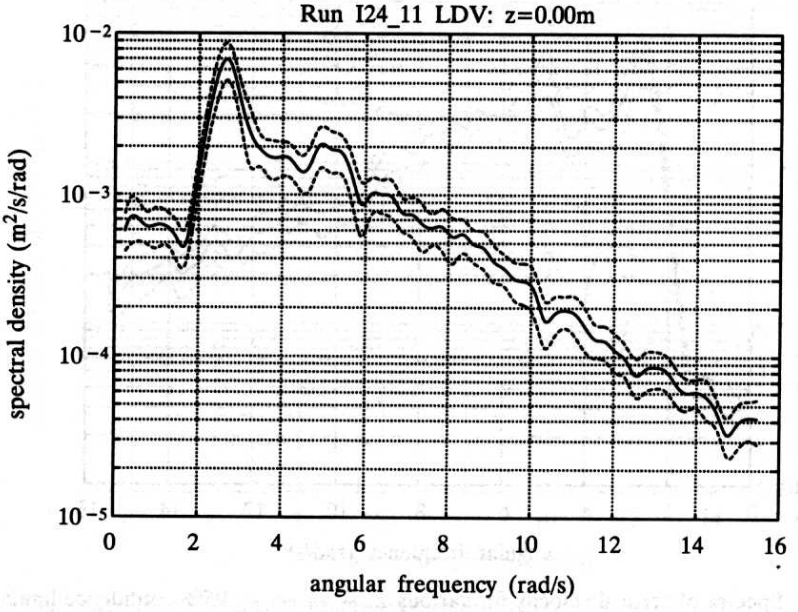


**Fig. 14b.** See Fig. 14a

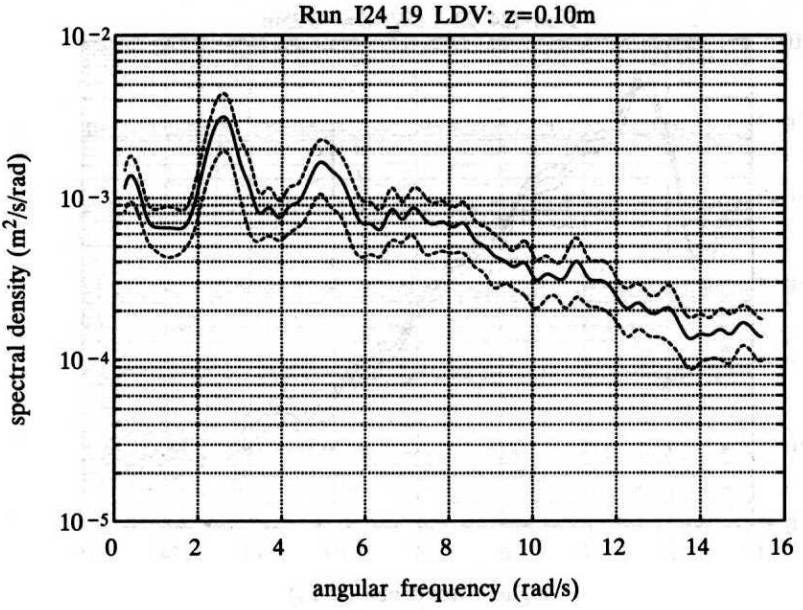


**Fig. 14c.** See Fig. 14a

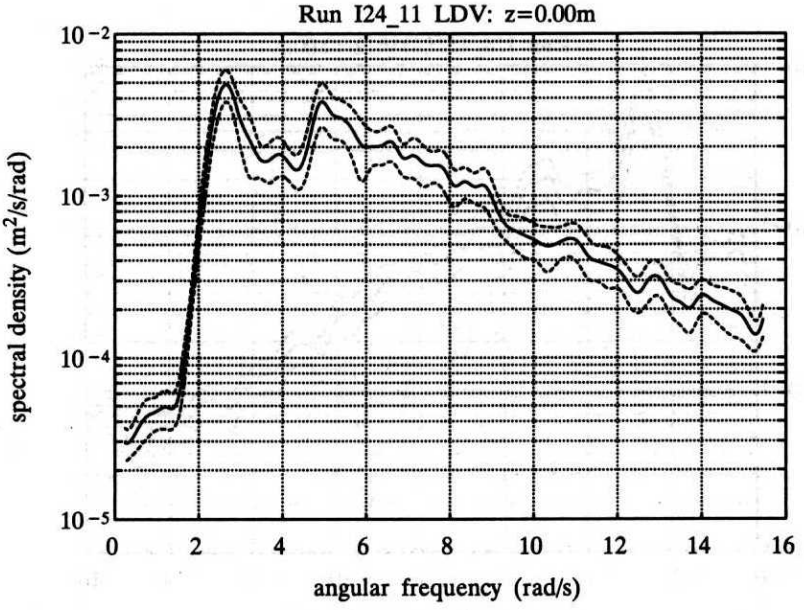


**Fig. 15a.** Spectra of vertical velocity for various $z$; – – – – 95% confidence limits. Wave case I24

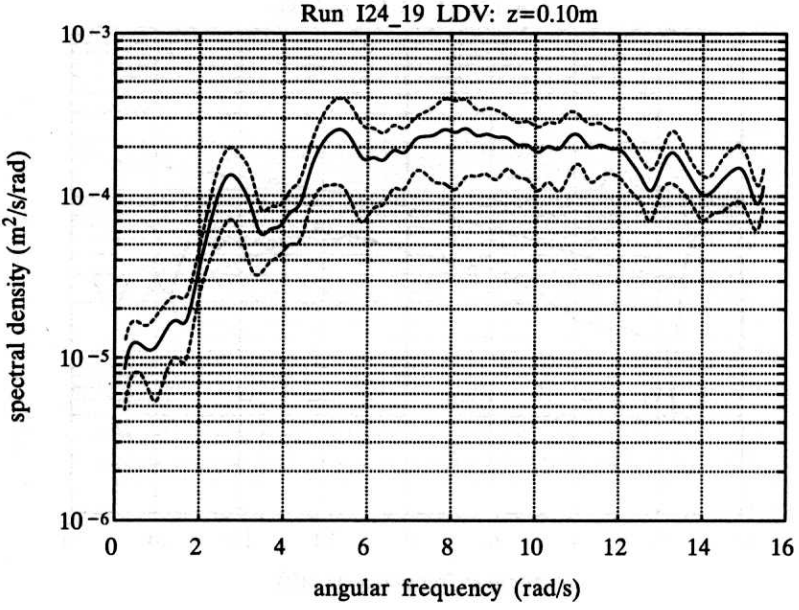


**Fig. 15b.** See Fig. 15a

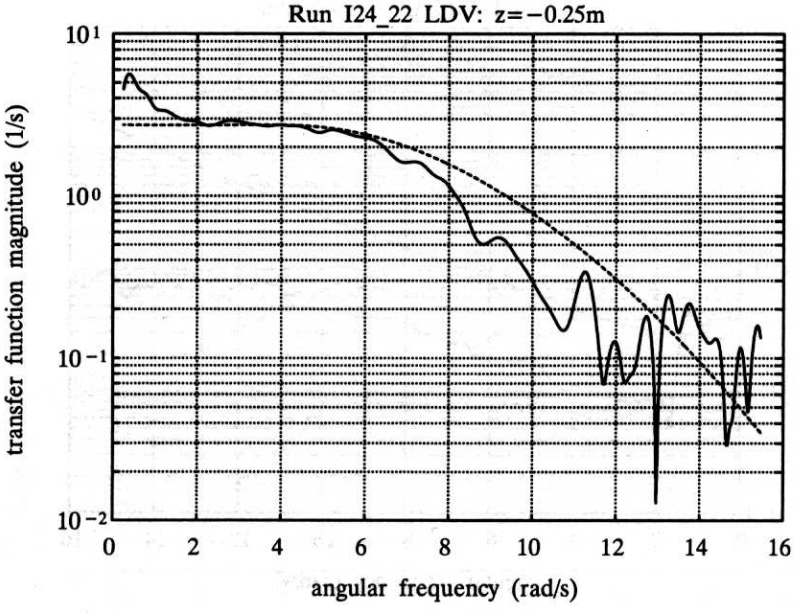


**Fig. 16a.** Magnitude of transfer function between surface elevation and horizontal velocity for various $z$; ———— observed, – – – – according to linear random wave theory. Wave case I24

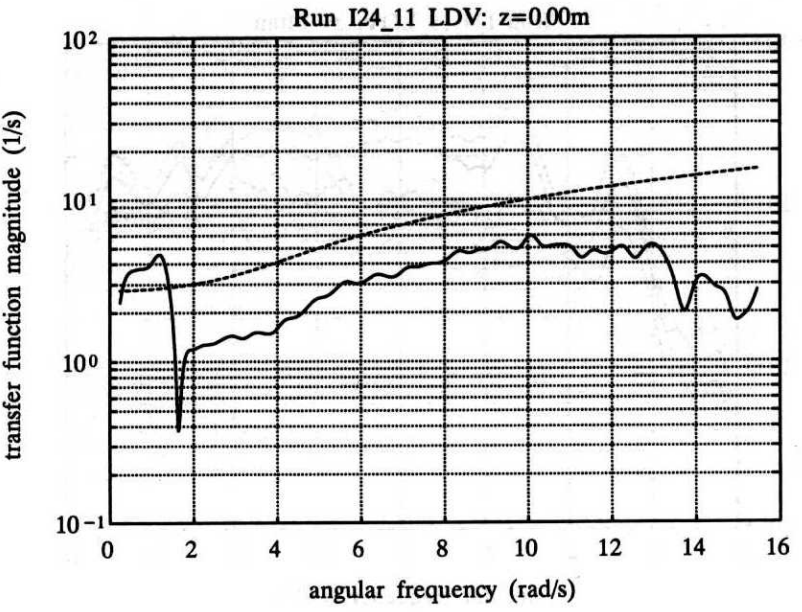


**Fig. 16b.** See Fig. 16a

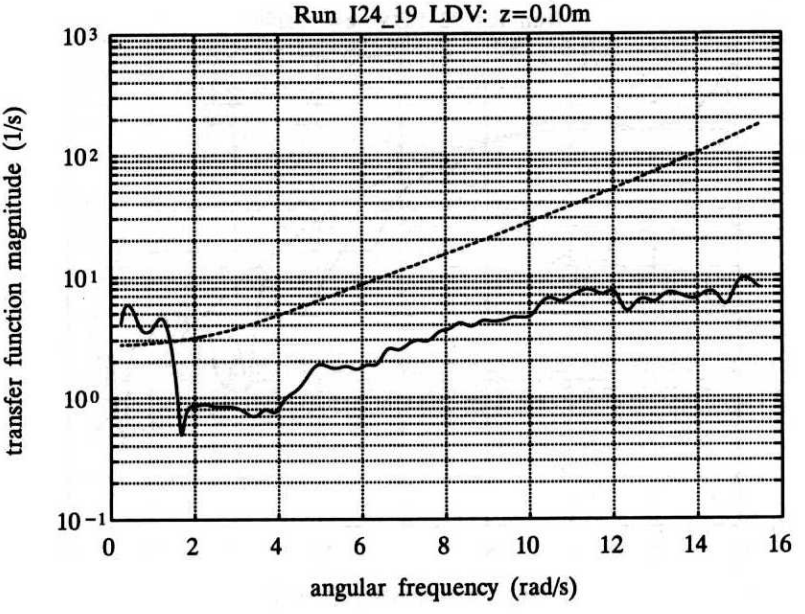


**Fig. 16c.** See Fig. 16a

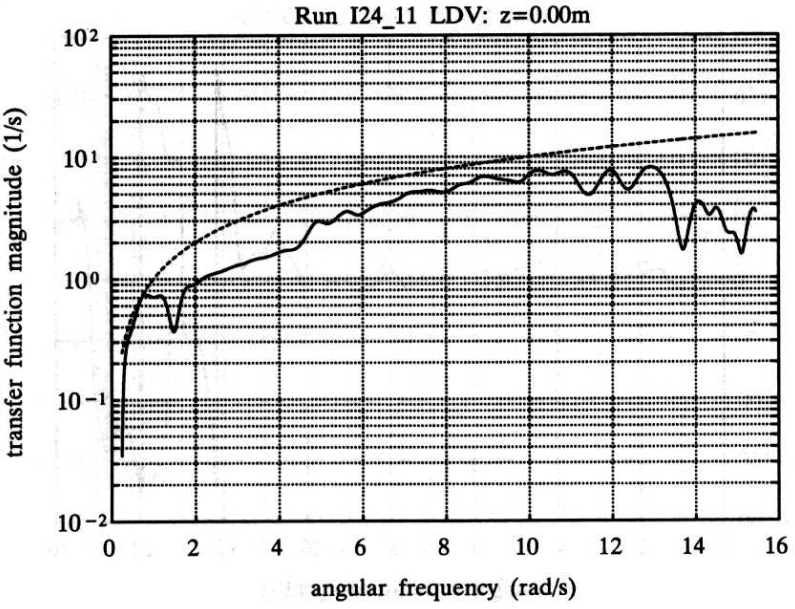


**Fig. 17a.** Magnitude of transfer function between surface elevation and vertical velocity for various $z$; ———— observed, – – – – according to linear random wave theory. Wave case I24

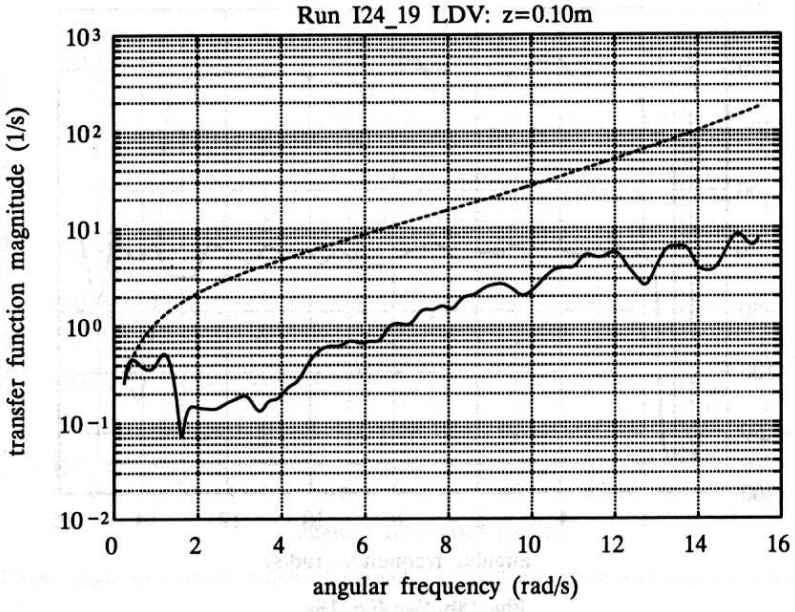


**Fig. 17b.** See Fig. 17a

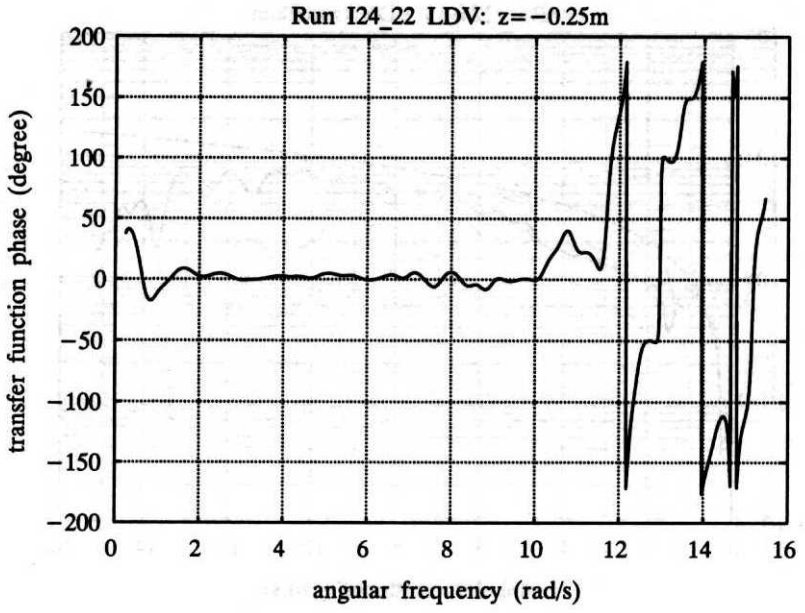


**Fig. 18a.** Phase angle of transfer function between surface elevation and horizontal velocity for various $z$. Wave case I24

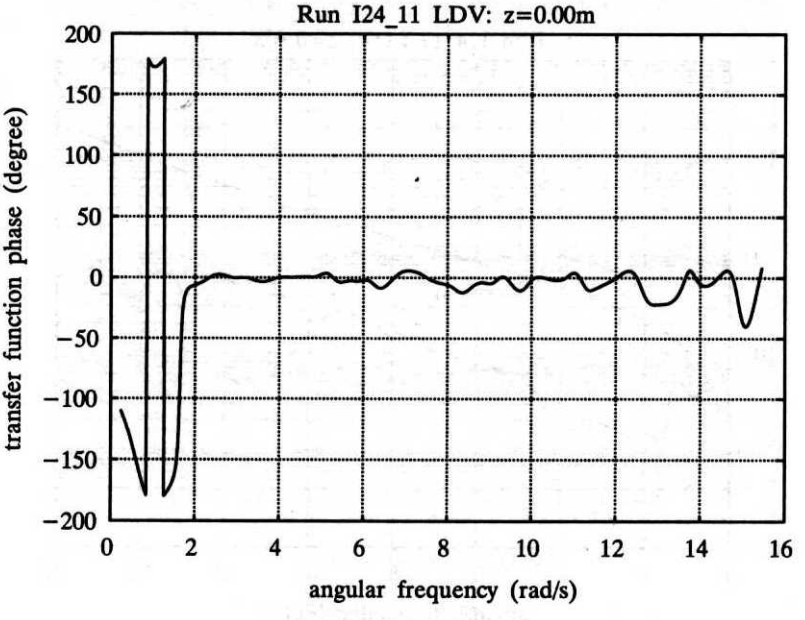


**Fig. 18b.** See Fig. 18a

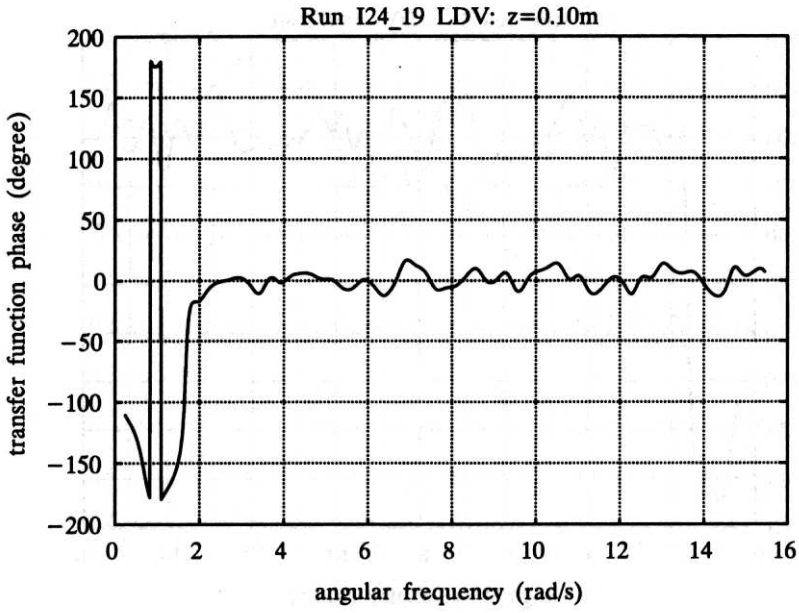


**Fig. 18c.** See Fig. 18a

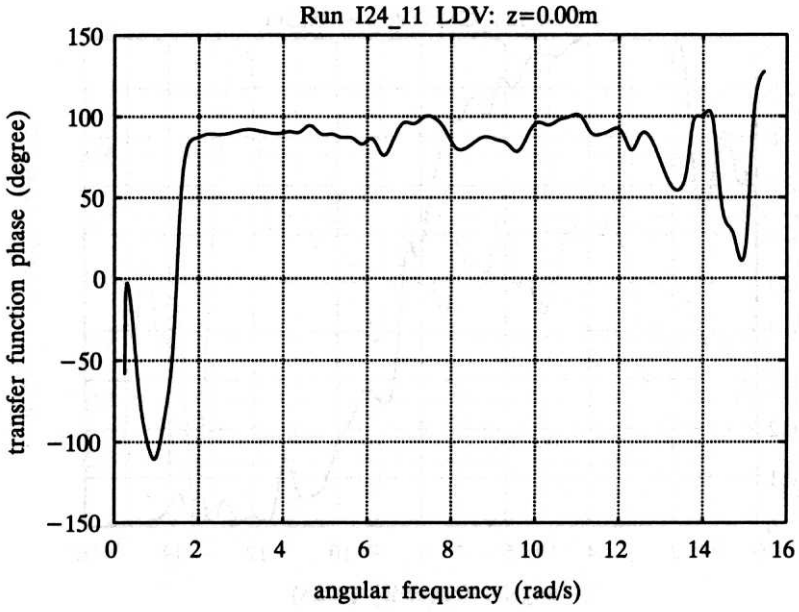


**Fig. 19a.** Phase angle of transfer function between surface elevation and vertical velocity for various $z$. Wave case I24

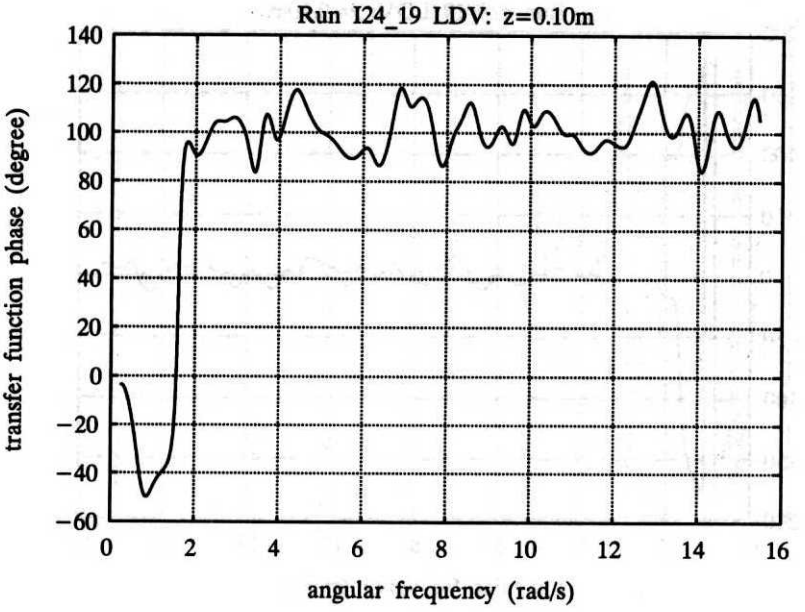


**Fig. 19b.** See Fig. 19a

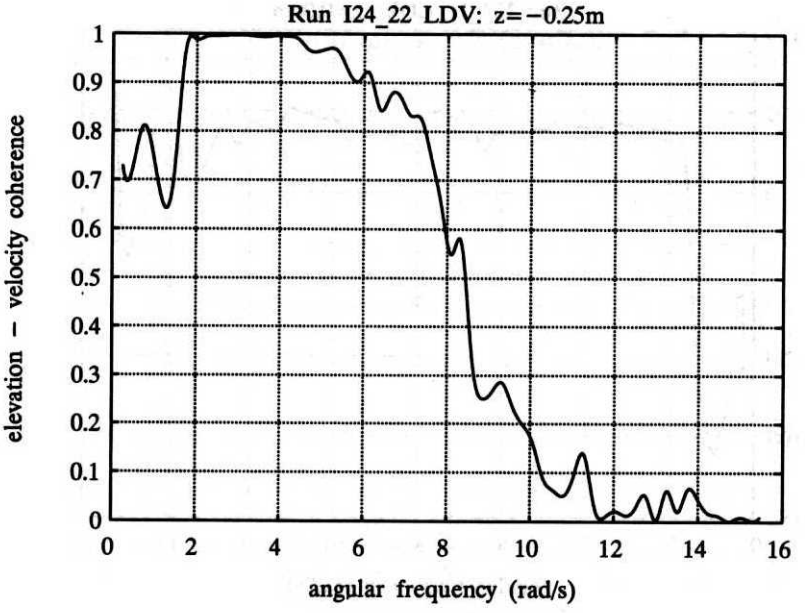


**Fig. 20a.** Coherence function between surface elevation and horizontal velocity for various $z$. Wave case I24

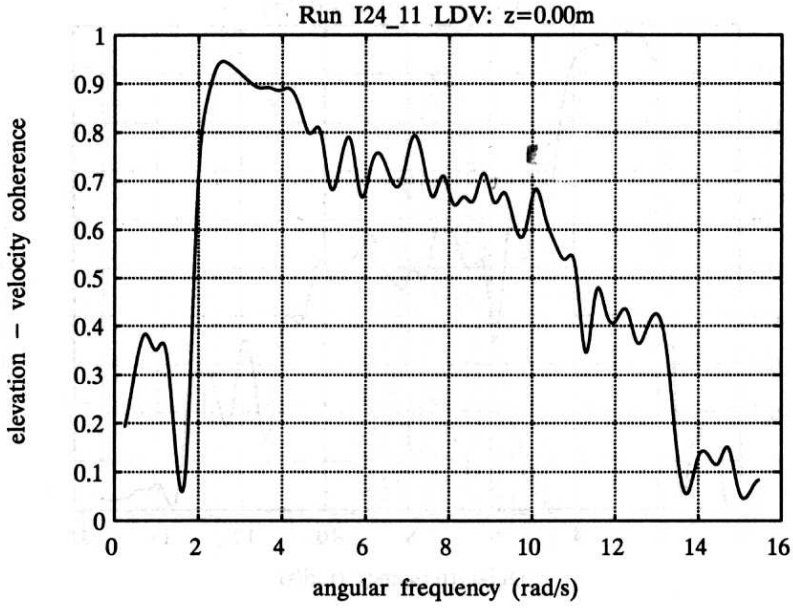


**Fig. 20b.** See Fig. 20a

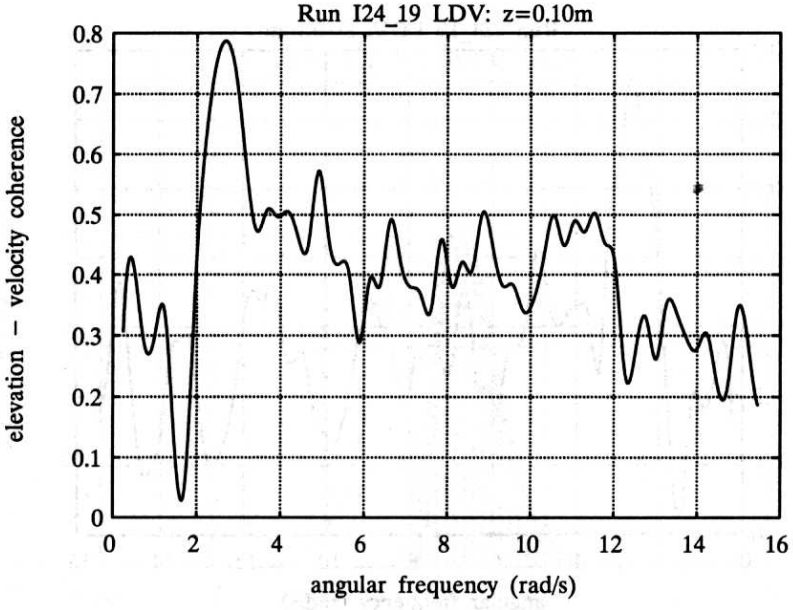


**Fig. 20c.** See Fig. 20a

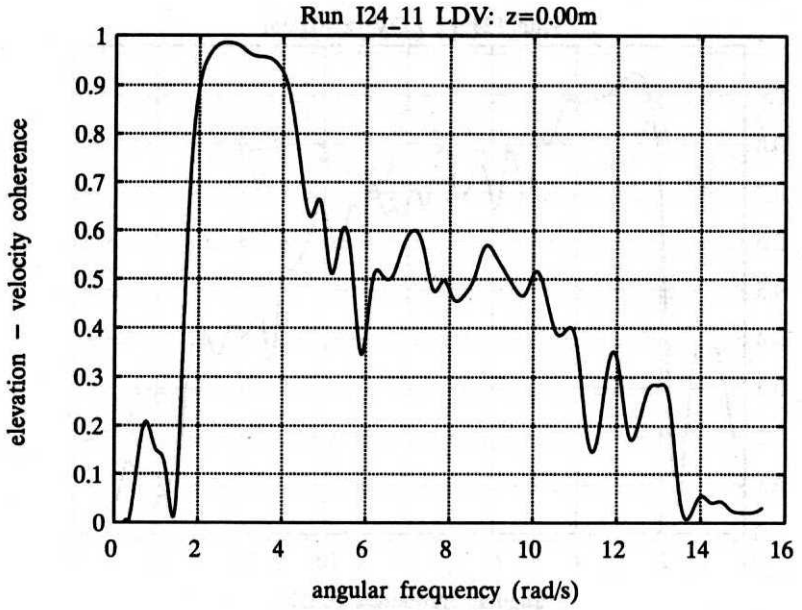


**Fig. 21a.** Coherence function between surface elevation and vertical velocity for various $z$. Wave case I24

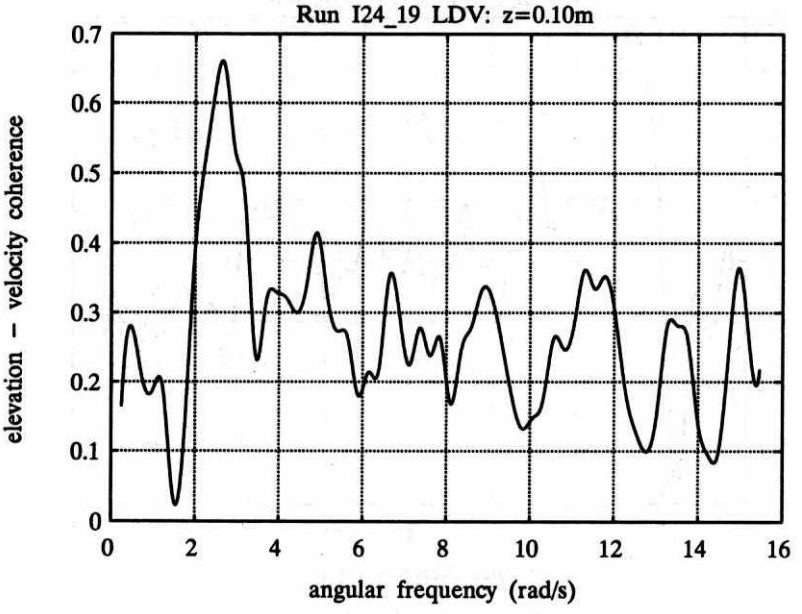


**Fig. 21b.** See Fig. 21a

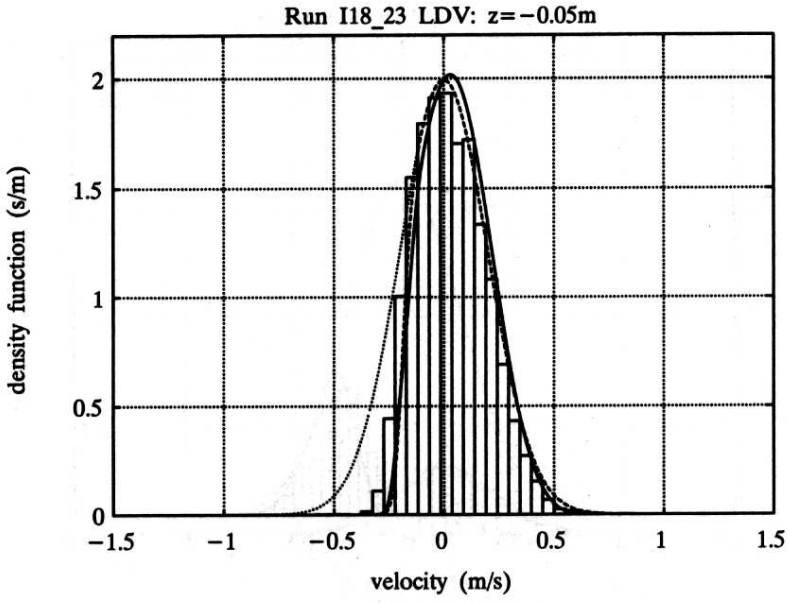


**Fig. 22a.** Continuous part of probability density function of horizontal velocity for various $z$; bar plot—observed values, ———— second-order according to (32)*, – – – – first-order according to (48)*, ····· first-order without emergence effect (Gaussian). Wave case I18

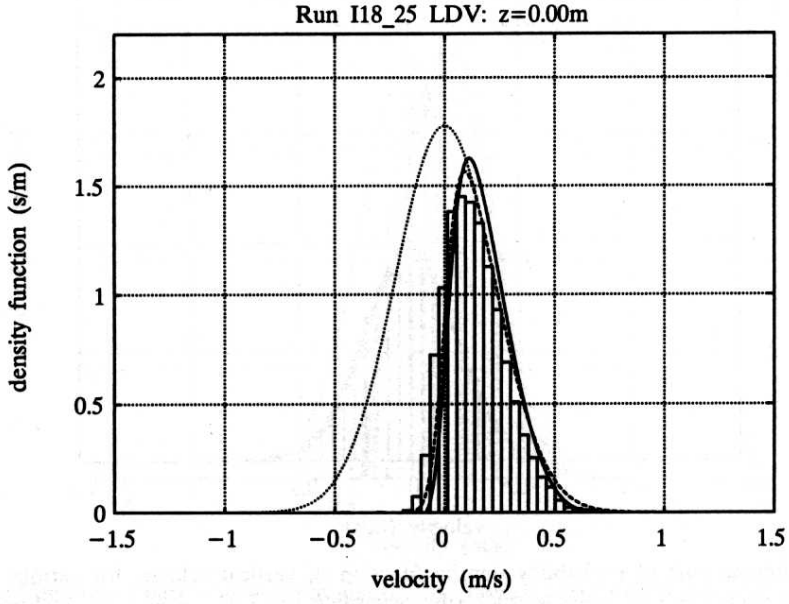


**Fig. 22b.** See Fig. 22a

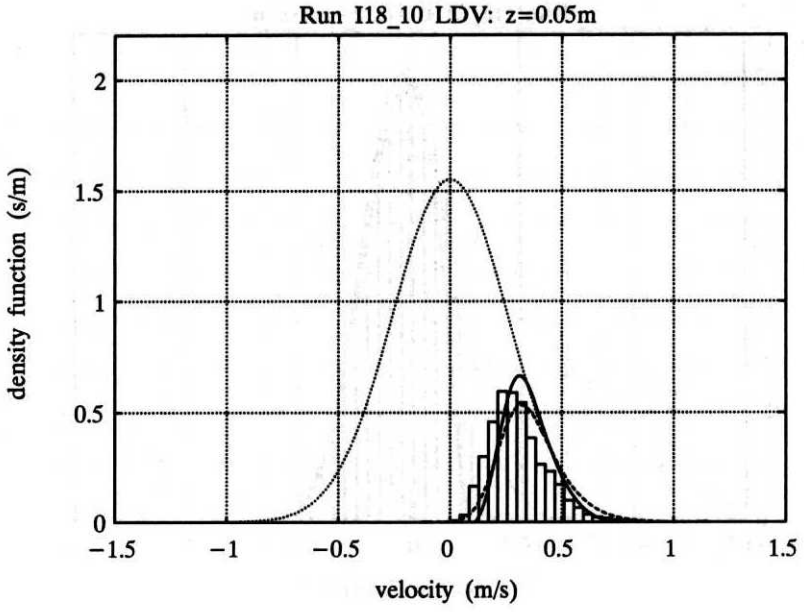


**Fig. 22c.** See Fig. 22a

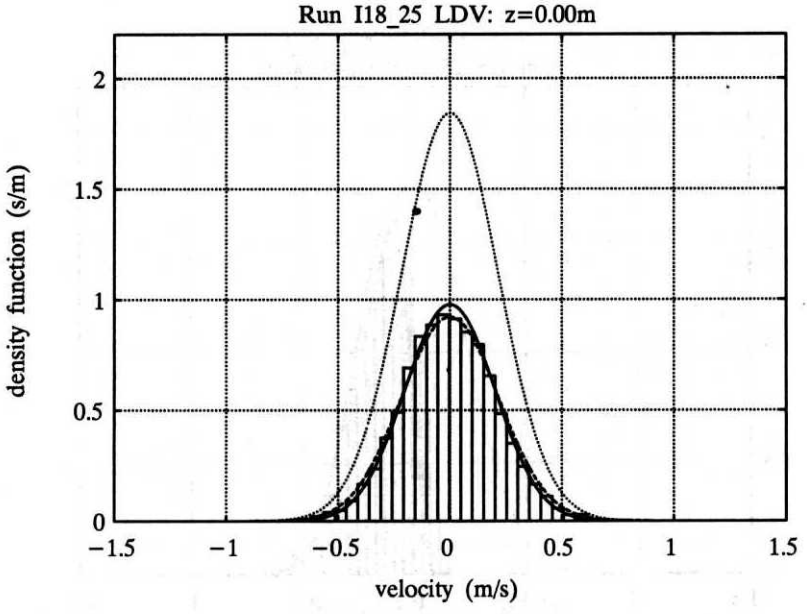


**Fig. 23a.** Continuous part of probability density function of vertical velocity for various $z$; bar plot—observed values, ———— second-order according to (32)*, – – – – first-order according to (48)*, ····· first-order without emergence effect (Gaussian). Wave case I18

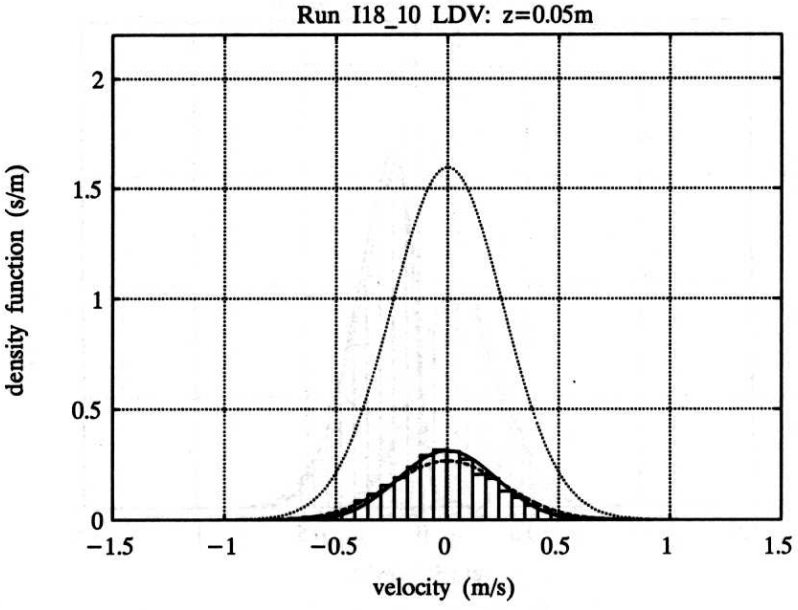


**Fig. 23b.** See Fig. 23a

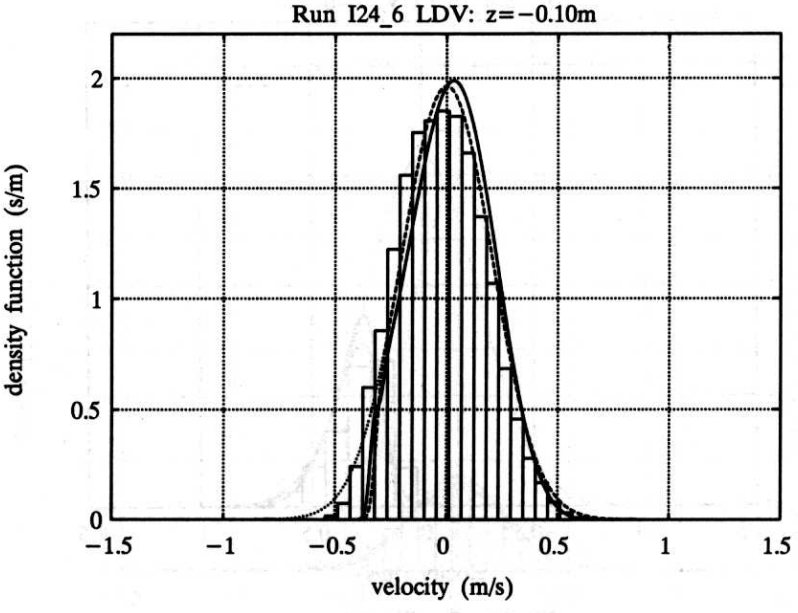


**Fig. 24a.** Continuous part of probability density function of horizontal velocity for various $z$; bar plot—observed values, ———— second-order according to (32)*, – – – – first-order according to (48)*, ····· first-order without emergence effect (Gaussian). Wave case I24

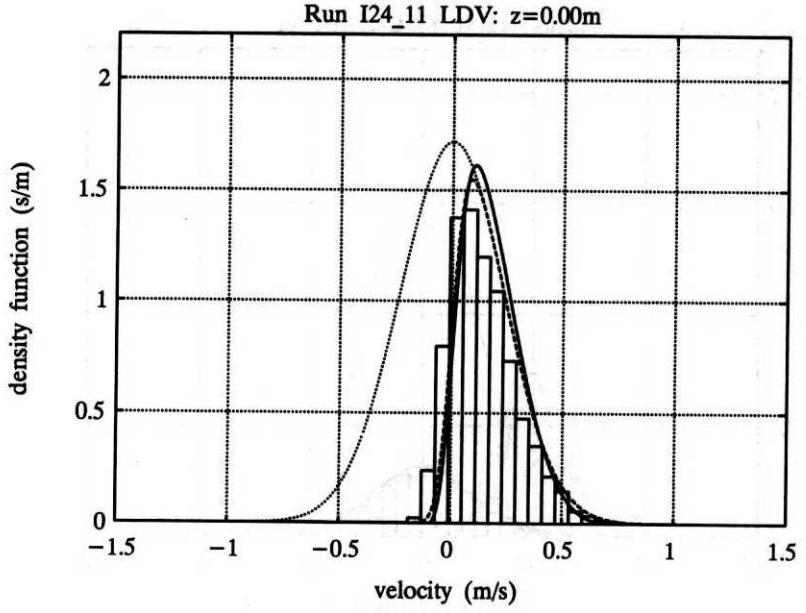


**Fig. 24b.** See Fig. 24a

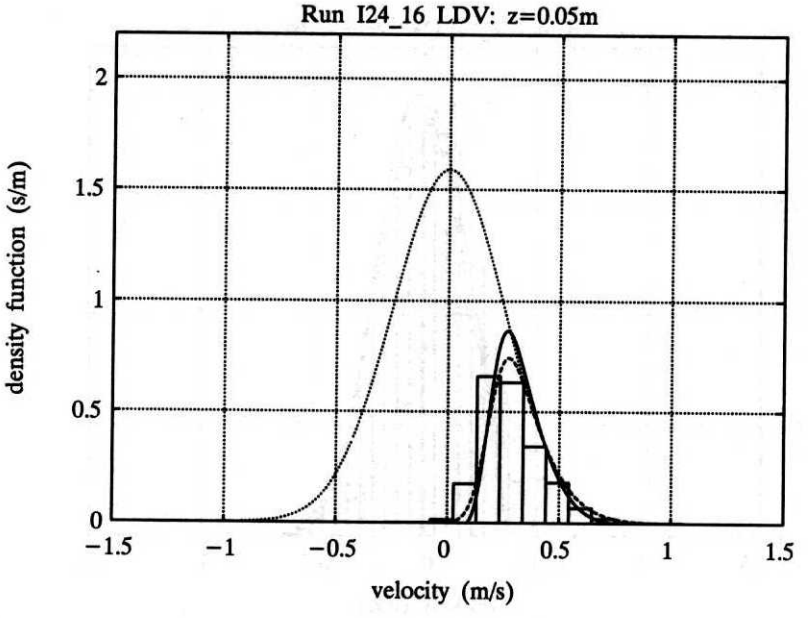


**Fig. 24c.** See Fig. 24a

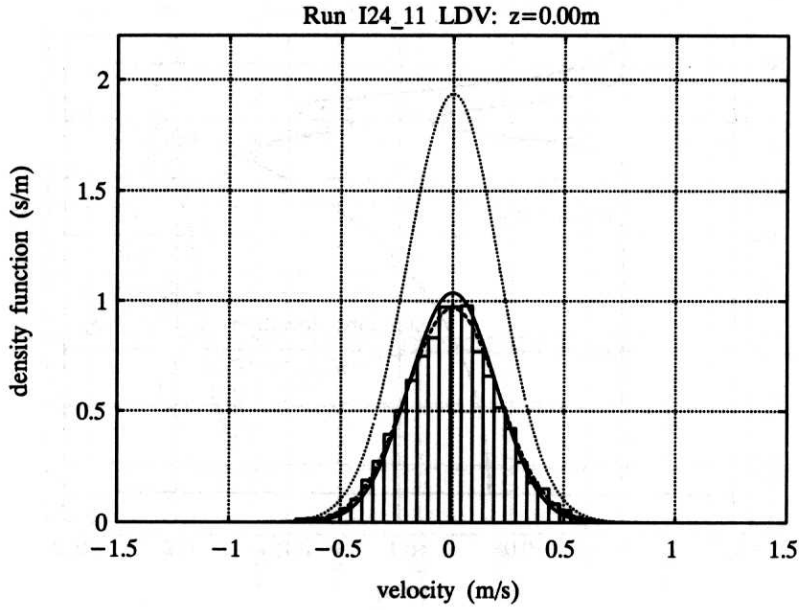


**Fig. 25a.** Continuous part of probability density function of vertical velocity for various $z$; bar plot—observed values, ———— second-order according to (32)*, – – – – first-order according to (48)*, ····· first-order without emergence effect (Gaussian). Wave case I24

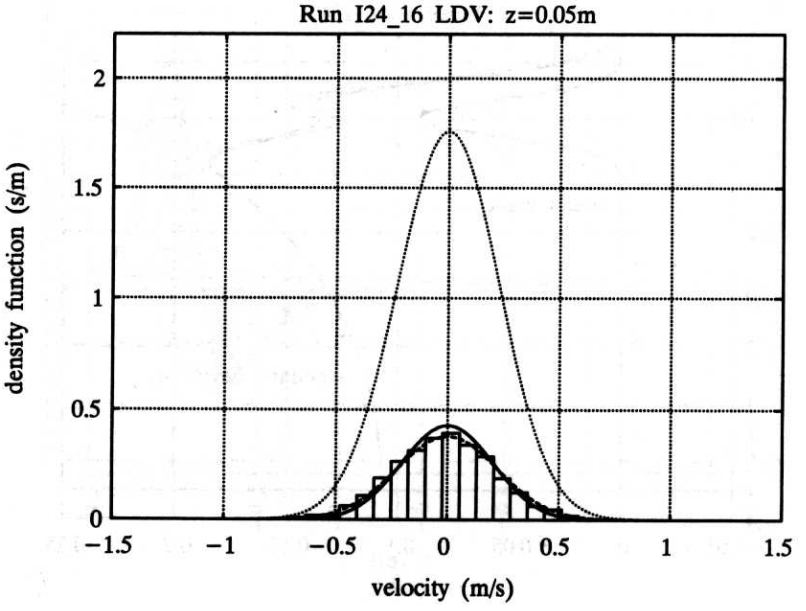


**Fig. 25b.** See Fig. 25a

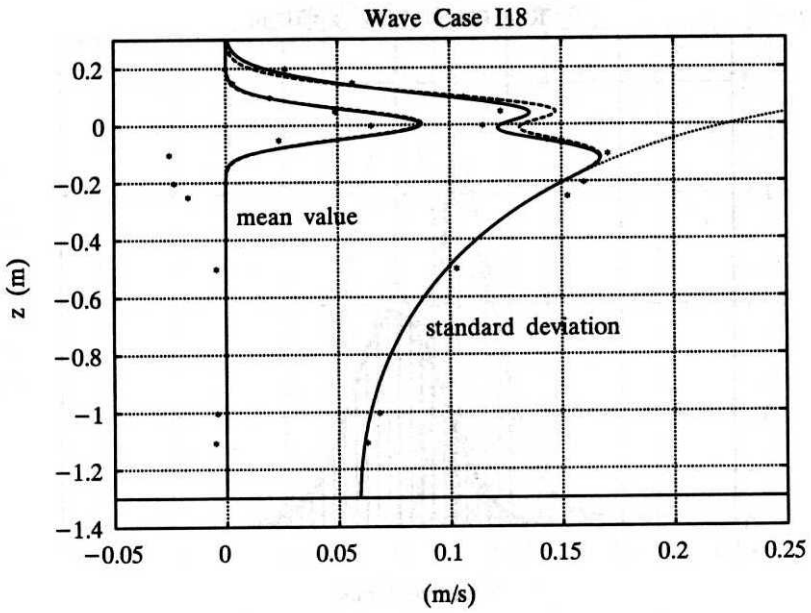


**Fig. 26a.** Mean value and standard deviation of horizontal velocity as functions of elevation $z$; $*$ observed values, ———— second-order, – – – – first-order, ····· first-order without emergence effect taken into account. a) Wave case I18, b) wave case I24

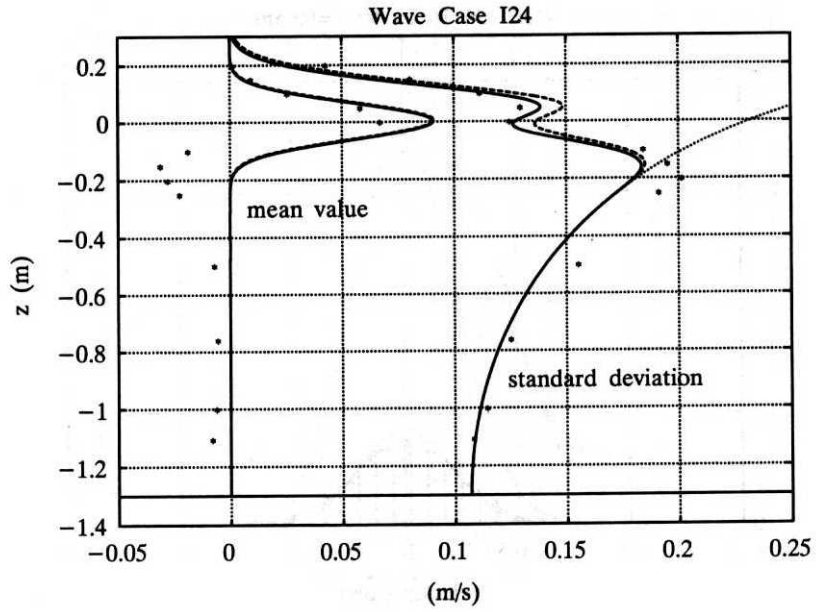


**Fig. 26b.** See Fig. 26a

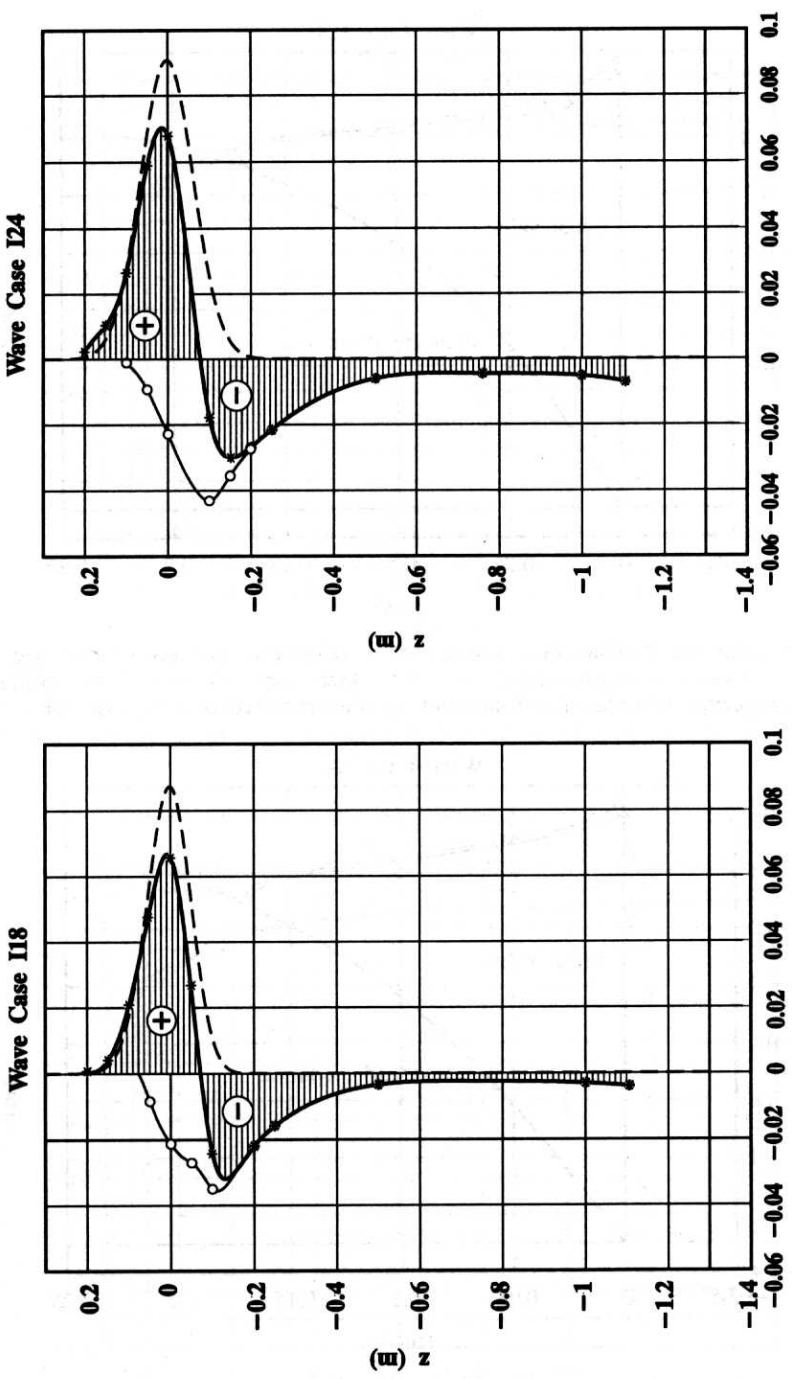


**Fig. 27.** Mean value of horizontal velocity and estimate of return flow: * observed mean values, – – – – according to formula (49)*, ○ estimated return flow. a) Wave case I18, b) wave case I24

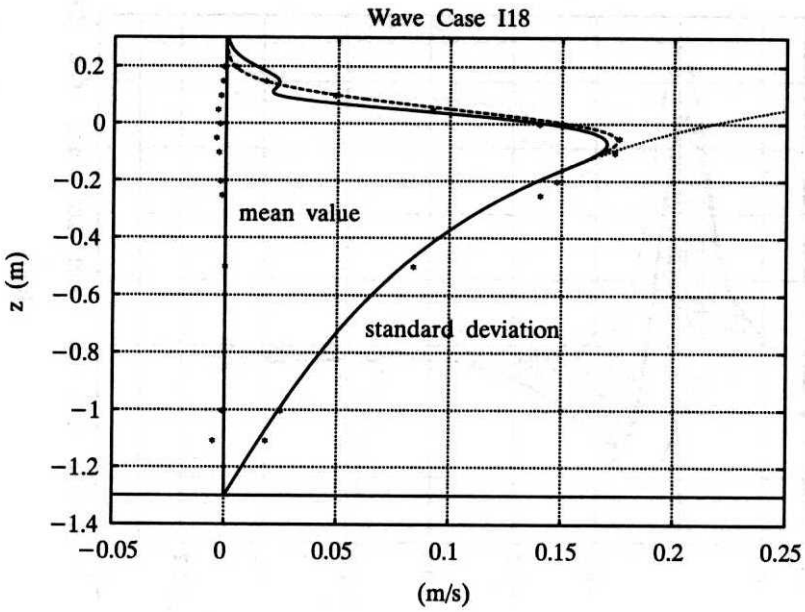


**Fig. 28a.** Mean value and standard deviation of vertical velocity as functions of elevation $z$; $*$ observed values, ———— second-order, – – – – first-order, ····· first-order without emergence effect taken into account. a) Wave case I18, b) wave case I24

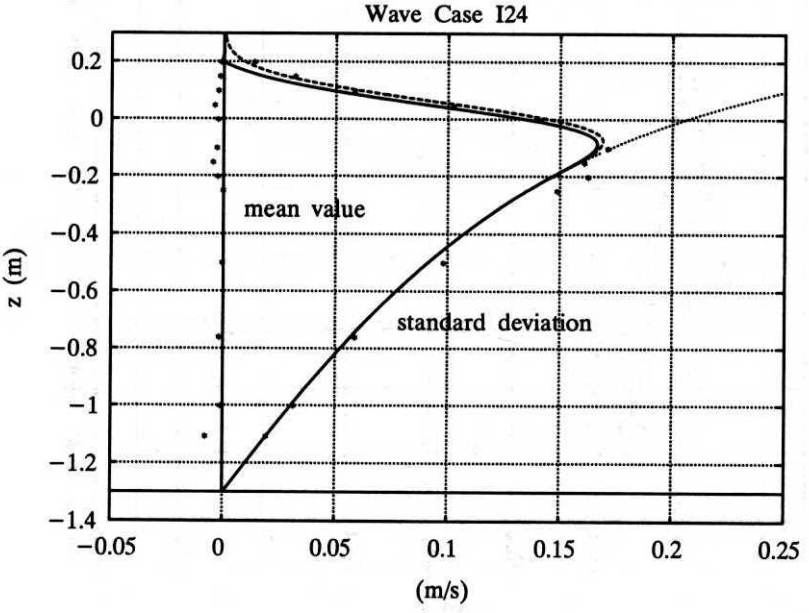


**Fig. 28b.** See Fig. 28a

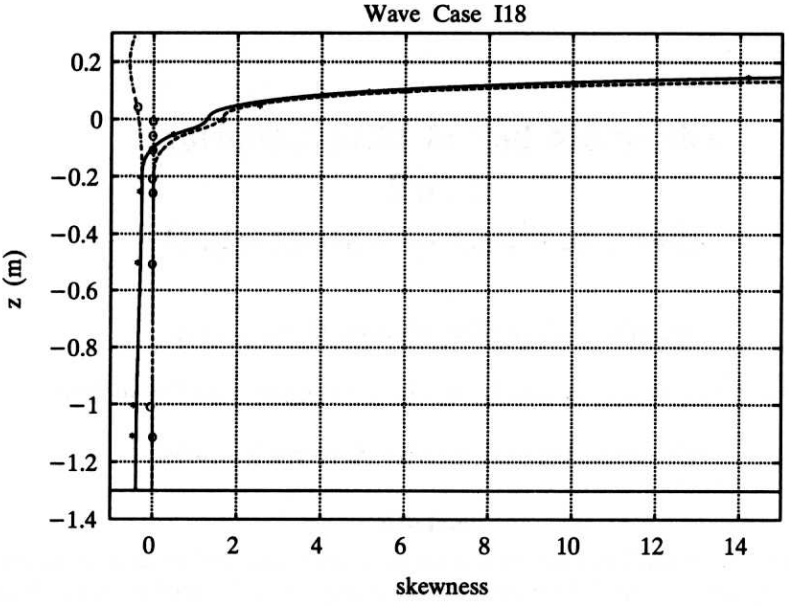


**Fig. 29a.** Skewness of particle velocity as function of elevation $z$; horizontal: ———— second-order, – – – – first-order, ·–·–·– second-order without emergence effect taken into account, ∗ observed values; ○ vertical observed values. a) Wave case I18, b) wave case I24

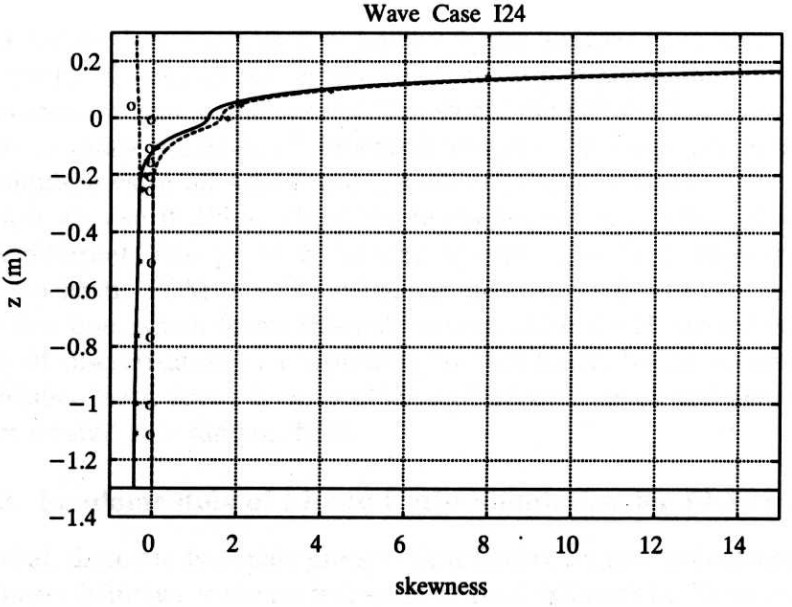


**Fig. 29b.** See Fig. 29a